Reactive Scattering and Resonance

4

Zhigang Sun, Bin Zhao, Shu Liu, and Dong-H. Zhang

Abstract

In this chapter, recent developments of the quantum wave packet methods for calculating differential cross sections (DCSs) of tetra-atomic reaction, for calculating DCSs of triatomic reaction using wave packet method only with reactant Jacobi coordinates, for calculating and analyzing the reactive resonance wave functions, and for simulating and explaining experimental observables of a reactive scattering, are given. Applications to the $F + H_2$ reaction, especially some fundamental understandings of its short-lived reactive resonances, the $H + O_2$ reaction, the $H_2 + OH \rightarrow H + H_2O$ reaction, and the $OH + CO \rightarrow H + CO_2$ reaction are presented for illustration.

4.1 Introduction

For decades it has been witnessed the persistent endeavors from both experimental and theoretical sides in the attempts to reveal the ever detailed minutes of how the reactants evolve to products during a chemical reaction process in various conditions. A chemical reaction may be envisioned as a scattering collision in which the original chemical bonds are cleaved and new ones are formed. Considering the large mass difference between electrons and nuclei, it is advantageous to separate the treatment of a reaction into solutions of two Schrödinger equations: first for the electrons at fixed nuclear positions, and then for the nuclei. This is the Born–Oppenheimer (BO) approximation, and it is valid for many chemical reactions. The treatment of the motions of electrons allows the definition of potential energy

Z. Sun (✉) • B. Zhao • S. Liu • D.-H. Zhang (✉)
State Key Laboratory of Molecular Reaction Dynamics and Center for Theoretical and Computational Chemistry, Dalian Institute of Chemical Physics, Chinese Academy of Sciences, Dalian 116023, China
e-mail: zsun@dicp.ac.cn; zhangdh@dicp.ac.cn

F. Gatti (ed.), *Molecular Quantum Dynamics*, Physical Chemistry in Action,
DOI 10.1007/978-3-642-45290-1_4,

surface (PES) as a function of all nuclear coordinates, and then the dynamic motions of nuclei during a reaction are governed by the PES, which provides the force acting on each nuclei in the system. A chemical reaction takes place on the PES along a minimum energy path connecting the reactant region to the product region, and it is called the reaction coordinate for the chemical reaction. In a typical chemical reaction, the path traverses a reaction intermediate region, which is defined as the transition state [34, 35].

Theoretically, the very early theory was pioneered by Hirschfelder and his coworkers dated back to the later 1930s and early 1940s [49, 52], but it takes more than 30 years to see the report of the fully quantum mechanical method on the simplest three-dimensional $H + H_2$ exchange reaction [110, 111], even though various model calculations were implemented on $H + H_2$ [62,108,109,133,134,143] and $F + H_2$ [106, 112, 144]. With the tremendous progress of various theoretical and numerical methods to deal with the partial differential equations and associated boundary conditions in the field of quantum reaction dynamics [4,15,50,90,96,107], it has now become just a routine to perform full-dimensional quantum scattering calculations for atom–diatom systems with both accurate ICS and DCS at the state-to-state level [3, 100, 119, 124, 140], especially after the introduction of reactant coordinate-based method [43, 126, 127]. Previously one had to transform the wave function between the reactant Jacobi coordinates and the product Jacobi coordinates (Jacobi coordinate is defined in Sect. 4.3), in order to efficiently express the reactant ro-vibrational states and the product ro-vibrational states and further obtain the state-to-state information. This leads to the well-known coordinate problem in time-dependent quantum wave packet calculation for extracting state-to-state reactive scattering information. Therefore quantum wave packet method had only been considered as a convenient method for calculating initial state-specific total reaction probabilities. Nowadays the quantumwave packet method has also been proved an effectivemethod for extracting state-to-state information.

Once the atom–diatom reactive scattering problem had essentially been solved, attention naturally turned to more complicated reactions involving more than three atoms—as the first step, to systems involving four atoms. Unfortunately, this is not a trivial task, as the number of degrees of freedom increases from three for a three-atom system to six for a four-atom system. In the past decades, significant progress has been made on accurate quantum reactive scattering studies of four-atom chemical reactions. Starting from time-independent (TI) reduced dimensionality approaches [15, 26], it is now possible to calculate fully converged integral cross sections [42, 155, 164], and state-to-state dynamical quantities for the total angular momentum $J = 0$ [29, 156, 165] without any dynamical approximation for some four-atom reactions, mainly through the development of the initial state selected wave packet method. Other quantum dynamical approaches have also received great success in four-atom reactions, such as the Multi-configurational Time-Dependent (TD) Hartree (MCTDH) approach for thermal rate constant calculations [72]. Various TID and TD reduced dimensionality calculations were also reported on different systems [118, 149, 154, 163, 166]. Recently, time-dependent wave packet (TDWP) method was developed to compute differential cross sections (DCSs) for

four-atom reactions and applied to the prototypical HD + OH → H_2O + D [70,145] and D_2 + OH → HOD + D reactions [69]. Excellent agreements were achieved for the first time for a four-atom reaction between the full-dimensional DCS and high-resolution crossed-molecular beam experimental results. Because it only takes a relatively short time to obtain fully converged DCS for the reaction, it is conceivable that the wave packet-based quantum scattering method has matured to the stage where it can afford yielding complete dynamical information for many four-atom reactions, as have been done for three-atom reactions in the past decades.

While fully quantum mechanical calculations on larger reactive system are always limited by the current computational power, the quasi-classical trajectory (QCT) method provides a feasible alternative by describing the scattering collisions with classical equations of motion [54, 99]. However, despite its high efficiency and intuitive nature, QCT is not a rigorous method to deal with quantum dynamics in reactive scattering, such as reactive resonance, zero-point energy, quantum tunneling, and interference. Even atoms other than hydrogen and its isotopes usually are not believed to have strong tunneling effect at room temperature, it is not clear what is exact the role of the zero-point energy in a molecular dynamics process.

In this chapter, we aim to provide quantum mechanical methods to simulate and explain some interesting experimental observables of reactive scatterings, especially some fundamental understandings of the short-lived reactive resonances.

4.2 Resonance in a Reactive Scattering

For a reactive scattering, the properties of the reaction system near the transient region have the dominant role that determines various details of reactive collisions including the nature of potential surfaces, nonadiabaticity, direct and complex-forming collision dynamics, energy partitioning, product state and angular distributions, quantum tunneling and resonances in the transient region, and other interference effects.

The literature has seen several comprehensive reviews that summarized the recent advances in the understanding of reactive resonance [22, 37, 66, 67, 148], and for the consideration of integrity, here we shall only briefly explain the basic concepts.

The properties of the reaction system near the transient region determine how the reactant evolves to the product side, and in a typical chemical reaction, reactions form short-lived intermediate reactive complex at the transition state region and finally decay into the final reaction products. The transition state region can be an energetic barrier, which separates the reactants from products, and in some cases after this barrier the reaction coordinate shows itself with a deep potential well, shown in Fig. 4.1a, which attracts the intermediate complex for a long time before it decays into the final products. The latter is always named as complex-forming reaction, and we shall not go into too much details in this kind of resonance, as recently it has been intensely reviewed by an elegant article [46]. We shall from now on only focus on the reactive resonance in direct reactions.

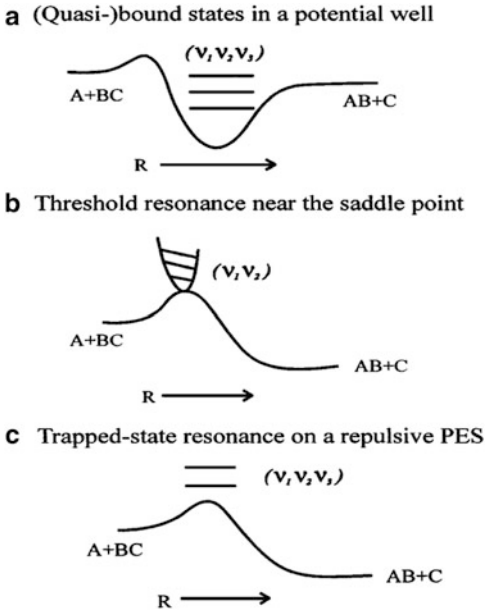

Fig. 4.1 Three types of reactive resonances near the transition state region in chemical reactions, adapted from [66]. Panel (**a**) illustrates the case associated with a deep potential well along the reaction coordinate. The resulting bound and pre-dissociative quasi-bound states can be characterized, for a three-atom system, by three vibrational modes. (**b**) Threshold resonance for which only the two motions orthogonal to the unbound reaction coordinate are quantized and thus assignable by vibrational quantum numbers. The dynamical trapped-state resonance is schematically shown in panel (**c**). Despite the repulsive potential energy surface along the reaction coordinate, this metastable state can be assigned by three vibrational quantum numbers

In a direct reaction, the minimum energy path along the reaction coordinate shows itself with repulsive feature on the PES, and no discrete quantum state exists in the transition state region along the reaction coordinate R, shown in Fig. 4.1b, c. The directions perpendicular to R are the internal coordinates $\mathbf{u}$ of the reaction system, and the motions along $\mathbf{u}$ are quasi-bound, which is the character of the saddle-point nature in the transition state region, shown in Fig. 4.1b. In a typical atom–diatom reaction, A + BC, the reaction coordinate approaches the asymmetric stretch motion of the ABC complex in the transition state region, and the two quasi-bound states are the symmetric stretching and bending modes. Due to the discrete nature of the two quasi-bound states, they would serve as a bottleneck to gate the flux going from the reactant region to product side. This is named as the threshold resonance or barrier resonance, and the discrete quasi-bound states are the quantized bottleneck states. As a result, stair-like feature is observed in the reaction probability $P_J(E_c)$ from a single partial wave J as a function of the collision energy, as shown in Fig. 4.2a (middle). The effect of zero-point energy manifests itself in the reaction probability as the smaller reaction threshold energy than the height of the barrier.

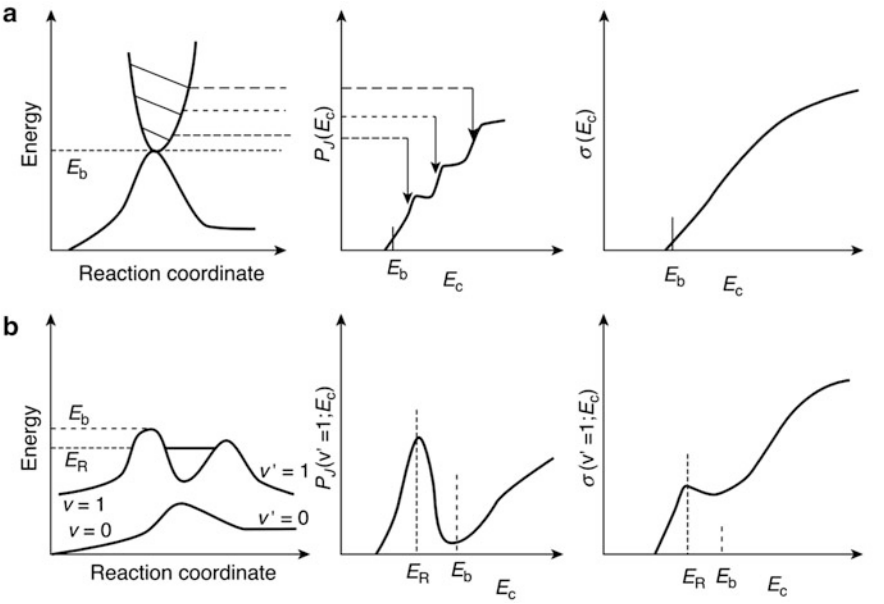

Fig. 4.2 Schematic illustration of the threshold resonances (**a**) and quantum dynamical resonance (**b**), adapted from [67]. In each panel, the *left figure* illustrates the effective dynamical potential along the reaction coordinate R, and the *middle* and the *right* ones are the E_c-dependence of the reaction probability $P_J(E_c)$ and the reaction cross section $\sigma(E_c)$. In the case of threshold resonance, the non-zero values of the reaction probability and cross section start at a smaller collision energy than the height of the barrier, which manifests the effect of zero-point energy

The other reactive resonance is called the trapped-state resonance or Feshbach resonance, shown in Fig. 4.1c. In this case, the ABC complex is dynamically trapped along the reaction coordinate, even the minimum energy path on the BO PES is totally repulsive. The trapping of the short-lived ABC complex is caused by the vibrationally adiabatic potential, which is based on the concept of vibrational adiabaticity [23, 75, 76, 120]. As the vibrational motions along the directions perpendicular to R are fast compared with the motion along R, the vibrational modes should approximately conserve the quantum number $\mathbf{n}$, which is in the spirit of BO separation of motions with different time scale. A typical vibrationally adiabatic potential along the reaction coordinate R is shown in Fig. 4.2b (left), and it can be constructed as

$$V_{\mathrm{VAP}}(R) = V_{\mathrm{MEP}}(R) + \varepsilon_{\mathbf{n}}(R) \tag{4.1}$$

in which $V_{\mathrm{MEP}}(R)$ is the minimum energy path along the reaction coordinate, and $\varepsilon_{\mathbf{n}}(R)$ is the quantized vibrational energy of the orthogonal motions. In the vicinity of the transition state region, the strong couplings between the vibrational motions and the reaction coordinate lead to the dramatic vibrational frequency

decrease due to the weakening of the bonds, and consequently dynamic potential well would appear along the reaction coordinate, especially for high vibrational quantum numbers. If the well is deep enough to support discrete resonance quantum state along the reaction coordinate, an isolated sharp peak should be observed in the reaction probability $P_J(E_c)$, as shown in Fig. 4.2b (middle) for $P_J(v' = 1; E_c)$ of the $v' = 1$ product state from a single partial wave J. The appearance of the isolated sharp peak before the reaction threshold energy is due to the resonant tunneling process through the barrier, which enhances the formation of the resonance complex state, and at higher collision energy, the direct reaction of the broad over-the-barrier probability dominates the process. In a one-dimensional model, the resonance produced by a potential like in Fig. 4.2b (left) is called as shape resonance [37]. While in multi-dimensional case, energy exchange occurs between various collective modes of the compound molecule, and it is named as the Feshbach resonace.

Even though the reaction probability provides distinctly different characteristics for the above two types of reactive resonance, the experimental observables of the reaction cross sections are often smeared out due to the summation of all possible $P_J(E_c)$, which is inevitable because of the existence of many partial. The interpretation of the experimental observables and further understanding of the effects of reactive resonance require the intense interplay between theory and experiment. For example, the transition state region is often tight, and only a small range of partial waves contributing to the DCS in certain direction, which is amenable to quantum mechanical calculations. We shall be able to focus on reaction probabilities of a certain range of partial waves, from which the different kinds of reactive resonance manifest themselves with distinct features.

In the following part, we will review the current quantum wave packet method for simulating reactive scattering processes and its applications, especially on understandings of reactive resonances. The quantum dynamical studies have greatly deepened our understandings of the reaction dynamics in some prototypical systems. The following part is full of technical details and one may skip it for a general interest.

4.3 Theory by Quantum Wave Packet Method

4.3.1 Overall Theory

In a reactive scattering, the full Hamiltonian H needs to be partitioned in different arrangement channels ν,

$$H = H_0^\nu + V^\nu \tag{4.2}$$

in which $H_0^\nu = T^\nu(R) + h^\nu(\boldsymbol{q})$ is the asymptotic Hamiltonian, V^ν is the interaction potential, and $T^\nu(R)$ is the kinetic energy operator in the translational degree of

freedom, R, $h^{\nu}(\boldsymbol{q})$ is the internal Hamiltonian in the internal degrees of freedom, $\boldsymbol{q}$. In the limit that the separation of the two fragments R goes to infinity, the interaction potential would be vanished, and the eigenfunction of the system is simply the product of a plane wave and the eigenfunction $\chi_n(\boldsymbol{q})$ of the internal Hamiltonian $h^{\nu}(\boldsymbol{q})$,

$$\psi^{\nu}_{n,E}(R,\boldsymbol{q}) = u^{\nu}_{k}(R)\chi^{\nu}_{n}(\boldsymbol{q}) \tag{4.3}$$

in which $\chi^{\nu}_{n}(\boldsymbol{q})$ is related to E_n by

$$h^{\nu}(\boldsymbol{q})\chi^{\nu}_{n}(\boldsymbol{q}) = E_n\chi^{\nu}_{n}(\boldsymbol{q}) \tag{4.4}$$

and the translational plan wave is directly written as

$$u^{\nu}_{k}(R) = \frac{e^{ikR}}{\sqrt{2\pi}} \tag{4.5}$$

where $k = \sqrt{2\mu(E-E_n)/\hbar^2}$, μ is the reduced mass of the translational motion. The eigenfunction $\psi^{\nu,\pm}_{n,E}$ of the full Hamiltonian H is related to the asymptotic wave function through the Møller operator, $\Omega_{\pm}$ [153],

$$\psi^{\nu,\pm}_{n,E} = \Omega_{\pm}\psi^{\nu}_{n,E} \tag{4.6}$$

Given the definition of S matrix operator, $S = \Omega^{\dagger}_{-}\Omega_{+}$, the probability amplitude to scatter from an initial state i of the reactant arrangement α to a final state f of the product arrangement β is written as the matrix element of the S operator [153],

$$S_{\beta f,\alpha i} = \langle\psi^{\beta}_{f,E}|S|\psi^{\alpha}_{i,E}\rangle = \langle\psi^{\beta}_{f,E}|\Omega^{\dagger}_{-}\Omega_{+}|\psi^{\alpha}_{i,E}\rangle = \langle\psi^{\beta,-}_{f,E}|\psi^{\alpha,+}_{i,E}\rangle \tag{4.7}$$

There are generally two methods to calculate the S matrix element. The first one is the time-independent (TI) method, which solves the eigenvalues of the full Hamiltonian H to obtain the scattering matrix $\psi^{\beta,-}_{f,E'}$ and $\psi^{\alpha,+}_{i,E}$. In a single run of the TI method, the entire S-matrix is obtained at a particular energy E. TI method is especially suitable for the case with low energy, such as cold collision problem. However, the TI method is notorious for its bad scaling relation N^3, with respect to the number of basis functions, N. Alternatively, the time-dependent (TD) method or wave packet method has a better scaling of N^2, and it is carried out by solving the TD Schrödinger equation of a first-order differential equation.

In a typical wave packet method, three steps are involved to calculate the S matrix. First, an initial wave packet Ψ_i of definite internal quantum states is launched in the reactant region with normally a Gaussian shape wave packet in the scattering coordinate, and this determines the range of collision energy. Then the wave packet is propagated for a sufficient length of time until the reaction is finished. Finally, the state-to-state S-matrix element is obtained for the reactive scattering. In the TD

method, the S-matrix element is reformulated by wave packet correlation function [132],

$$S_{\beta f,\alpha i} = \frac{(2\pi\hbar)^{-1}}{a_f^*(E)a_i(E)} \int_0^\infty e^{iEt/\hbar} \langle \Psi_f | e^{-iHt/\hbar} | \Psi_i \rangle dt \tag{4.8}$$

where Ψ_f is the final wave packet, $a_i(E)$ and $a_f(E)$ are the energy amplitudes of the energy normalized eigenfunctions contained in the initial and final wave packets. It can be seen that the S matrix element is obtained by the Fourier transform of the time correlation function $C_{fi}(t)$ between the final wave packet and the propagated initial wave packet, $C_{fi}(t) = \langle \Psi_f | \Psi_i(t) \rangle$.

It should be noted that the initial and final wave packets are usually expressed in the Jacobi coordinates of their own arrangements, which results in the difficult coordinate problem in state-to-state reactive scattering as we mentioned previously. One may either choose the product Jacobi coordinate [47, 53, 65, 151], or reactant Jacobi coordinate to propagate the initial wave packet, and there also exist two other methodologies but may be both named as reactant coordinate-based (RCB) method: the first one is to employ interpolation schemes for the coordinate transformation [41, 89, 126, 127, 156], and the second one is realized by projection of both reactant and product wave packets to an intermediate coordinate [43, 127], Alternatively, in the reactant–product decoupling (RPD) method [6, 7, 96], both the reactant and product coordinates are used, and they are divided and combined by a complex absorbing potential.

4.3.2 Quantum Wave Packet Method

The ever increasing popularity of the wave packet approach to reactive scattering is attributed largely to its intuitive time dependence and better scaling laws [87]. However, the concept of wave packet was originally postulated long time ago by Schrödinger in 1926 [115] as a coherent superposition of states, with localization in its position representation. The states can be electronic states, vibrational states, or rotational states, but in molecular wave packet method, the wave packet represents the coherent nuclei motion on certain electronic PES under Born–Oppenheimer approximation. Since the formulation of these original works, molecular wave packet theory has undergone a huge development, as reviewed by Manz in his comprehensive historical survey of molecular wave packet theory in the period of 1926–1996 [74].

Since the numerical details for a triatomic reactive scattering can be directly extended to more complicated systems and are very typical, we will focus on the triatomic reactions in this part.

4.3.2.1 Hamiltonian and Discretization

To study the atom–diatom reactive scattering, $\mathrm{A} + \mathrm{BC}(v_i, j_i) \rightarrow \mathrm{AB}(v_f, j_f) + \mathrm{C/AC}(v_f, j_f) + \mathrm{B}$ at a state-to-state level, body-fixed (BF) frame Jacobi coordinates are

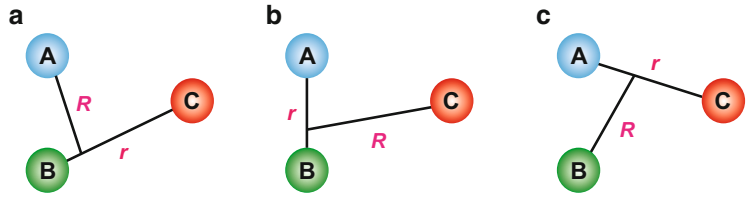

Fig. 4.3 The Jacobi coordinates for the reactant A + BC (**a**), and product AB + C (**b**) and AC + B (**c**)

used to represent the corresponding wave packets in their arrangements: normally the reactants A + BC is for the α arrangement, and the two product channels AB + C and AC + B are for the β and γ arrangements, respectively. The Jacobi coordinates for the three arrangements are shown in Fig. 4.3. In each arrangement, the coordinate is denoted as $(R_v, r_v, \theta_v; \boldsymbol{\Omega_v})$, where v represents any one of the above arrangements. For example, when v represents the reactant arrangement, R_v is the length of vector $\boldsymbol{R}_v$ pointing from the BC center of mass to A, r_v the BC bond length, and θ_v the angle between BC bond and $\boldsymbol{R}_v$; $\boldsymbol{\Omega_v}$ denotes the Euler angles orienting $\boldsymbol{R}_v$ in the space-fixed (SF) frame.

Considering the reaction scattering as an isolated system, the calculation is always carried out using a partial wave representation, in which the total angular momentum J is a good quantum number and one can take advantage of the conservation of the total angular momentum to break the problem into separate calculations for each value of the total angular momentum quantum number J. The Hamiltonian for a given total angular momentum $\boldsymbol{J}$ is given in the reactant Jacobi coordinate as

$$\hat{H} = -\frac{\hbar^2}{2\mu_R}\frac{\partial^2}{\partial^2 R} - \frac{\hbar^2}{2\mu_r}\frac{\partial^2}{\partial^2 r} + \frac{\hat{l}^2}{2\mu_R R^2} + \frac{\hat{j}^2}{2\mu_r r^2} + V(R, r, \theta) \tag{4.9}$$

where the arrangement label α is removed for clarity consideration, μ_R and μ_r are the corresponding reduced mass for R and r, respectively. The squared orbital angular momentum operator is responsible for the centrifugal potential and expressed as

$$\hat{l}^2 \equiv (\hat{\boldsymbol{J}} - \hat{j})^2 = \hat{\boldsymbol{J}}^2 + \hat{j}^2 - 2\hat{\boldsymbol{J}}_z\hat{j}_z - \hat{\boldsymbol{J}}_+\hat{j}_- - \hat{\boldsymbol{J}}_-\hat{j}_+ \tag{4.10}$$

where $\hat{\boldsymbol{J}}$ and $\hat{j}$ are the total and BC diatomic rotational angular momentum operators, with $\hat{\boldsymbol{J}}_z$ and $\hat{j}_z$ as their corresponding projections onto the BF z-axis, which coincides with the vector $\mathbf{R}$. The raising/lowering operators in the last two terms, $\hat{\boldsymbol{J}}_\pm$ and $\hat{j}_\pm$, represent the Coriolis coupling, which couples the adjacent helicity quantum number K. K is the projection of both J and j onto the BF z-axis, and it is a good quantum number in the BF frame.

For each partial wave J and parity ϵ, the Hamiltonian and wave packet are discretized in the BF frame in mixed representation [21, 64, 80, 89, 160]: discrete variable representation (DVR) is employed for the two radial degrees of freedom and finite basis representation (FBR) of normalized associated Legendre function $\mathscr{Y}_{jK}(\theta)$ for the angular degree of freedom. Thus the wave packet in the BF frame is written as

$$\Psi^{JM\epsilon}(\boldsymbol{R}, \boldsymbol{r}) = \sum_{K} \mathscr{D}^{J\epsilon *}_{MK}(\boldsymbol{\Omega}) \psi(t, R, r, \theta^K; K) \tag{4.11}$$

where $\mathscr{D}^{J\epsilon *}_{MK}(\boldsymbol{\Omega})$ is the parity-adapted normalized rotation matrix, depending only on the Euler angles $\boldsymbol{\Omega}$,

$$\mathscr{D}^{J\epsilon *}_{MK}(\boldsymbol{\Omega}) = (1 + \delta_{K,0})^{-1/2} \sqrt{\frac{2J+1}{8\pi}} [D^{J*}_{MK}(\boldsymbol{\Omega}) + \epsilon(-1)^{J+K} D^{J*}_{M-K}(\boldsymbol{\Omega})], \tag{4.12}$$

where ϵ is the parity of the system defined as $\epsilon = (-1)^{j+l}$ with l being the orbital angular momentum quantum number, and $D^{J*}_{MK}(\boldsymbol{\Omega})$ is Wigner rotation matrix [16, 152]. The usage of the parity-adapted normalized rotation matrix restricts the K to be nonnegative and the basis size is reduced almost by half. $\psi(t, R, r, \theta^K; K)$ only depends on three internal coordinates and K, and it is expanded as

$$\psi(t, R, r, \theta^K; K) = \sum_{n,m,j} F^K_{nmj}(t) u_n(R) \phi_m(r) \mathscr{Y}_{jK}(\theta) \tag{4.13}$$

where n and m are the radial basis labels, $u_n(R)$ and $\phi_m(r)$ are the corresponding basis functions, respectively, and $\mathscr{Y}_{jK}(\theta)$ is the normalized associated Legendre function.

4.3.2.2 Construction of the Initial Wave Packet

As has been mentioned above, the first step of the wave packet method is to set up the initial wave packet. The initial wave packet is advantageous to be defined in the SF frame, because the Coriolis couplings in the BF frame are long ranged and it requires to define the initial wave packet at rather large position of R. There are not many ways to account for them in a reasonable grid. On the other hand, in the SF frame, the asymptotic form of the scattering wave function can be described by the Riccati–Hankel function, and the long-range centrifugal term is diagonal, $l(l+1)/2\mu_R R^2$ [3, 30]. Consequently, the initial wave packet can be placed as close as the interaction potential is negligible. In such a manner, the initial wave packet is defined as the product of the diatomic ro-vibrational eigenstate $\phi_{v_0 j_0}(r)$ of BC and a Gaussian wave packet $G(R)$ in the translational coordinate [3, 65, 126],

$$\Psi^{JM\epsilon}_{v_0 j_0 l_0}(\boldsymbol{R}, \boldsymbol{r}) = G(R) \phi_{v_0 j_0}(r) |JM j_0 l_0 \epsilon\rangle, \tag{4.14}$$

where $|JMj_0l_0\epsilon\rangle$ is the eigenfunction of the total angular momentum operator in the coupled representation of the SF frame with parity of system $\epsilon = (-1)^{j_0+l_0}$, and the Gaussian wave packet $G(R)$ in the translational coordinate is given as

$$G(R) = \left(\frac{2}{\pi\delta^2}\right)^{1/4} e^{-(R-R_0)^2/\delta^2} e^{-ik_0R}, \tag{4.15}$$

in which δ, R_0, and k_0 are the width, mean position, and mean momentum of the translational wave packet, respectively, and they determine the range of collision energy.

Wave packet is always propagated in the BF frame, and the initial wave packet needs to be transformed from the SF to the BF frames before the propagation, which is to transform the SF eigenfunction $|JMj_0l_0\epsilon\rangle$ of the total angular momentum operator in the coupled representation to the BF frame,

$$\begin{aligned} |JMj_0l_0\epsilon\rangle &= \sum_{K\geq 0} \boldsymbol{C}_{l_0K}^{Jj_0\epsilon} |JMj_0K\epsilon\rangle \\ &= \sum_{K\geq 0} \boldsymbol{C}_{l_0K}^{Jj_0\epsilon} D_{MK}^{J\epsilon*}(\boldsymbol{\Omega}) \mathscr{Y}_{j_0K}(\theta), \end{aligned} \tag{4.16}$$

where $\boldsymbol{C}_{l_0K}^{Jj_0\epsilon}$ is the parity-adapted orthogonal transform matrix between the SF and BF frames [65, 101, 153, 157] and given as

$$\boldsymbol{C}_{l_0K}^{Jj_0\epsilon} = \sqrt{\frac{2l+1}{2J+1}} \sqrt{2-\delta_{K,0}} \langle jKl0|JK\rangle, \tag{4.17}$$

where $\langle jKl0|JK\rangle$ is the Clebsch–Gordan coefficient.

4.3.2.3 Propagation of the Wave Packet

After the preparation of the initial wave packet, it is then propagated under the operation of system Hamiltonian by the unitary propagator $U(t, t_0) = e^{-\frac{i}{\hbar}H(t-t_0)}$.

Usually, the propagator $U(t, t_0)$ is approximated by various schemes [55,60,137], and there are plenty of wonderful articles that have explained each in detail, such as the split operator method and higher order split operator methods [11, 36, 130], Chebyshev polynomial expansion [131], Faber polynomial expansion [51, 146], short iterative Lanczos propagation method [95], Crank–Nicholson second-order differencing [10, 56, 57], symplectic method [14, 45], recently proposed real Chebyshev method [24, 44, 125], and Multi-configuration Time-Dependent Hartree (MCTDH) Method [12, 73, 81–83]. For details, one may refer to the corresponding references.

4.3.3 State-to-State Method: The RPD Approach

It has been a long time that only the product Jacobi coordinates were used in the propagation for extracting state-to-state information: the initial wave function, which is constructed in reactant Jacobi coordinate, is first transformed into product Jacobi coordinate, directly or after some propagation time to focus the initial wave packet in interaction region. Then the wave function propagation and product state-resolved information is calculated. Later, RPD method was proposed [96], particularly for direct reactive scattering process where it has been proved being very efficient. Recently, efficient RCB method was put forward by Sun et al. and Roncero et al. [43, 126, 127], particularly for reactive scattering process involving intermediate complex. The RCB method has been applied with $H + O_2$ [124], $O + O_2$ [128], $N + NO \rightarrow N_2 + O$ etc., which clearly demonstrated its efficiency and convenience for usage. In this part we only briefly introduce the RPD method, which is the only technique capable of extracting state-to-state DCS of tetra-atomic molecules currently.

The RPD method, originally introduced by Peng and Zhang [96] in order to extract the state-to-state information efficiently, transforms no-return part of reacted wave packet continuously in time from reactant to product coordinates with the help of absorption potentials. It divides the full time-dependent wave function into the reactant and product components and the calculation of each component can be carried out using the Jacobi coordinates of the corresponding arrangement channel separately. The RPD method solves, to a large extent, the problem of the choice of coordinates in quantum reactive scattering.

In the time domain, the RPD scheme partitions the full time-dependent (TD) wave function into a sum of reactant component (Ψ_r) and all product components (Ψ_p, $p = 1, 2, 3, \ldots$) that satisfy the following decoupled equations:

$$
\begin{aligned}
i\hbar\frac{\partial}{\partial t}|\Psi_r(t)\rangle &= H|\Psi_r(t)\rangle - i\sum_p V_p|\Psi_r(t)\rangle \\
i\hbar\frac{\partial}{\partial t}|\Psi_p(t)\rangle &= H|\Psi_p(t)\rangle + iV_p|\Psi_r(t)\rangle,
\end{aligned}
\tag{4.18}
$$

where $-iV_p$ is the negative imaginary potential (absorption potential) used to prevent the wave function $\Psi_r(t)$ from entering the pth product arrangement. The solution for $\Psi_r(t)$ is independent of those for $\Psi_p(t)$ and the latter are independent of each other. Therefore, $\Psi_r(t)$ can be propagated in the reactant Jacobi coordinates just as for total reaction probability calculations,

$$
\Psi_r(t + \Delta) = e^{-V_p\Delta/\hbar}e^{-(i/\hbar)H\Delta}\Psi_r(t). \tag{4.19}
$$

Every product wave function, Ψ_p, can be propagated in its own coordinates as in a normal wave packet propagation except with a source term, ξ_p, provided by Eq. (4.19),

$$\Psi_p(t+\Delta) = e^{-(i/\hbar)H\Delta}\Psi_p(t) + \xi_p(t) = e^{-(i/\hbar)H\Delta}\Psi_p(t) + (1 - e^{-V_p\Delta/\hbar})\Psi_r(t+\Delta). \tag{4.20}$$

Finally, one can extract the final state information, such as state-to-state S matrix elements or reaction probabilities, from the Fourier transformation of $\Psi_p(t)$.

The RPD approach is very efficient on dealing with direct reactants with barriers as demonstrated by Althorpe and coworkers [3, 8], because in this case the absorption potential can be applied right after the barrier as in initial selected total reaction probability calculations and it is also rather cheap to carry out the continuous propagation for the absorbed wave packet in a product channel. In particular, Althorpe and coworkers have realized that the absorption of reacted wave packet can be performed after multiple propagation steps [5, 29].

In the original RPD approach, the source term $\xi_p(t) = (1 - e^{-V_p\Delta/\hbar})\Psi_r(t)$ is saved and transformed from reactant to product Jacobi coordinates at every propagation time step. By using the multiple-step reactant–product decoupling (MRPD) scheme, one can be saving and transforming the source term at every M time [68, 70, 71].

$$\begin{aligned}
&\Psi_r(t+\Delta) = e^{-V_pM\Delta/\hbar}e^{-(i/\hbar)H\Delta}\Psi_r(t), \text{ when } \mathrm{mod}((t+\Delta) - t_0, M\Delta) = 0,\\
&\Psi_p(t+\Delta) = e^{-(i/\hbar)H\Delta}\Psi_p(t) + (1 - e^{-V_pM\Delta/\hbar})\Psi_r(t+\Delta),
\end{aligned} \tag{4.21}$$

where t_0 is the starting point for performing wave function transformation. At other time steps, we carried out the standard split-operator propagation for $\Psi_r(t)$ and $\Psi_p(t)$ without the absorption potential, V_p, related terms. In this way, we can cut the computational time for wave function transformation from reactant coordinates to product coordinates by a factor of M.

Since the efficiency of RPD method for a state-to-state calculation of a direct reactive scattering process, it is crucial for extracting product state-resolved information of tetra-atomic reaction limited by current computer resource. The applications below of tetra-atomic reaction are accomplished by using the RPD method.

4.3.4 Calculation of the Experimental Observations

4.3.4.1 Calculation of S-Matrix of Triatomic Reaction Using the RCB Method

To calculate the state-to-state S-matrix in Eq. (4.8), the time correlation function $C_{fi}(t) = \langle\Psi_f|\Psi_i(t)\rangle$ needs to be calculated at each time step during the propagation. A projection plane is often defined as $R_\nu = R_{\nu 0}$ for the νth ($\nu = \beta$ or γ) arrangement using the corresponding product Jacobi coordinate, and the time correlation function is always carried out on this projection plane but the projection action can be carried out in either reactant or product Jacobi coordinate. The final product wave packet $\Psi_f(R_\nu)$ is also defined in the SF frame due to the merits already mentioned above,

$$\begin{aligned}\Psi_f^{JM\epsilon}(R_{v0}) &\equiv \Psi_{v_v j_v l_v}^{JM\epsilon}(\boldsymbol{R}', \boldsymbol{r}') \\ &= \delta(R' - R_{v0})\phi_{v_v j_v}(r')|JMj_v l_v \epsilon\rangle \\ &= \delta(R' - R_{v0})\phi_{v_v j_v}(r') \sum_{K' \geq 0} \boldsymbol{C}_{l_v K'}^{J j_v \epsilon} D_{MK'}^{J\epsilon *}(\boldsymbol{\Omega}') \mathscr{Y}_{j_v K'}(\theta') \end{aligned} \tag{4.22}$$

in which R', r', and θ' describe the product Jacobi coordinate, and $\boldsymbol{\Omega}'$ are the Euler angles for $\boldsymbol{R}'$ in the SF frame. In practice, one often calculates the scattering wave function in the energy domain before taking overlap with the final product state, and it is obtained by a time-energy Fourier transform from the propagated wave packet,

$$\Phi_i^{JM\epsilon}(E; R_{v0}) = \int_0^\infty e^{iEt/\hbar} \Psi_i^{JM\epsilon}(t; R_{v0}) dt, \tag{4.23}$$

With the strategy to deal with the coordinate problem as mentioned in Sect. 4.3.1, the state-to-state S-matrix can be readily evaluated,

$$S_{v_v j_v l_v \leftarrow v_0 j_0 l_0}^{J\epsilon}(E) = \frac{(2\pi\hbar)^{-1}}{a_f^*(E) a_i(E)} \langle \Psi_f(R_{v0}) | \Phi_i^{JM\epsilon}(E; R_{v0}) \rangle \tag{4.24}$$

where $a_i(E)$ and $a_f(E)$ are given by

$$a_i(E) = \left(\frac{\mu_R}{2\pi\hbar^2 k_{v_0 j_0}} \right)^{1/2} \int \mathscr{H}_{l_0}(k_{v_0 j_0} R) G(R) dR \tag{4.25}$$

$$a_f(E) = \left(\frac{\mu_{R'}}{2\pi\hbar^2 k_{v_v j_v}} \right)^{1/2} \mathscr{H}_{l_v}(k_{v_v j_v} R_{v0}) \tag{4.26}$$

in which $\mu_{R'}$ is the reduced mass for the product translational degree of freedom, $\mathscr{H}_l$ is the outgoing Riccati–Hankel function.

Finally, the S-matrix needs to be transformed from the SF frame to the helicity representation by the standard transformation,

$$S_{v'j'K' \leftarrow vjK}^J = \sum_{l'l} i^{l-l'} \sqrt{\frac{2l'+1}{2J+1}} \langle j'K'l'0|JK' \rangle S_{v'j'l' \leftarrow vjl}^J \sqrt{\frac{2l+1}{2J+1}} \langle jKl0|JK \rangle. \tag{4.27}$$

4.3.4.2 Calculation of ICS and DCS

By substituting the S-matrix $S_{v'j'K' \leftarrow vjK}^J(E)$ in the helicity representation into the standard formulas, the state-to-state ICS can be obtained by summing over the contributions from all partial waves [157],

$$\sigma_{v_v j_v \leftarrow v_0 j_0}(E) = \frac{\pi}{(2j_0+1)k^2_{v_0 j_0}} \sum_{K_v} \sum_{K_0} \sum_{J} (2J+1) |S^{J\epsilon}_{v_v j_v K_v \leftarrow v_0 j_0 K_0}(E)|^2 \tag{4.28}$$

and the state-to-state DCS [157],

$$\frac{d\sigma_{v_v j_v \leftarrow v_0 j_0}(\vartheta, E)}{d\Omega} = \frac{1}{(2j_0+1)} \sum_{K_v} \sum_{K_0} \left| \frac{1}{2ik^2_{v_0 j_0}} \sum_{J} (2J+1) d^J_{K_v K_0}(\vartheta) S^{J\epsilon}_{v_v j_v K_v \leftarrow v_0 j_0 K_0}(E) \right|^2, \tag{4.29}$$

in which ϑ is the scattering angle between the direction of incoming reactant A and outgoing product AB/AC in the center of mass frame, and $d^J_{K_v K_0}(\vartheta)$ is the reduced rotational matrix [16, 152].

4.3.4.3 Calculation of Reaction Rate

With the calculated initial state-specific ICS, the initial state-specific temperature-dependent reaction rate constant can be expressed as

$$k(T|v_0 j_0) = \left(\frac{8K_b T}{\pi \mu_R}\right)^{1/2} (k_b T)^{-2} \int_0^\infty dE \exp\left(\frac{E_t}{k_b T}\right) \sigma_{v_v j_v \leftarrow v_0 j_0}(E) \tag{4.30}$$

where k_b is Boltzmann's constant. The thermal rate constant can be calculated from the Boltzmann averaging of the initial state-specific reaction rate constants as

$$k(T) = Z_{\text{elec}}(T) \frac{\sum_{v_0 j_0} (2j_0+1) k(T|v_0 j_0) \exp(-E_{v_0 j_0}/(k_b T))}{\sum_{v_0 j_0} (2j_0+1) \exp(-E_{v_0 j_0}/(k_b T))} \tag{4.31}$$

where $E_{v_0 j_0}$ is the ro-vibrational energy of the reactant diatomic molecule, and $Z_{\text{elec}}(T)$ is the possible electronic partition function for the system.

For a reaction with a defined transition state and without recrossing, reaction rate can be well approximated by many methods. For such reaction, we can assume that there is a dynamics bottleneck located at the transition state (conventional transition state theory, TST) or at a generalized transition state obtained by a canonical (CTV) or microcanonical (μVT) criterion. In the later cases, the dividing surface is optimized variationally to minimize the recrossing. Evans first proposed to place the transition state at the location that maximizes the free energy of activation which provides a key conceptual framework for modern variational transition state theory [33]. However, recrossing always possibly exists and only a full-dimensional reactive scattering dynamics calculations are able to provide us the exact rate constant on a defined PES. For a detailed discussion, one may refer to the reviews by Truhlar et al. [38, 136].

4.3.4.4 Calculation and Characterization of the Reactive Resonance Wavefunction

It is crucial to characterize the features of the reactive resonance wave function, in order to understand the nature and role of a particular reactive resonance state in the reaction.

The nomenclature "resonance" refers to a transient metastable species produced in the reaction scattering processes, and it results in peaks in the plots of reaction probabilities as a function of collision energy. Although its observation and assignment in scattering experiments usually is difficult because the coherent summation of many partial waves tends to wash out most of the resonance structures, numerically the quantum calculation is carried out with a specified partial wave and the resonance is much easier to pick out. The existence signature of a dynamical resonance is the arising of a peak in the collision energy-dependent reaction probability enhanced by the metastable transient state with long enough lifetime. Thus, such dynamical resonance wavefunctions can be figured out by using the so-called spectral quantization method. The bottleneck state in the $H + H_2$ and its isotopes reactions scattering processes [104] and the reactive resonance state in the $F + HD$ reaction processes [116] have been investigated using the spectral quantization method. In that method a carefully designed initial wave function was applied to obtain the time-independent wave function at the peak energies in the reaction probabilities by Fourier transform of the time-propagated wave packet. The reactive resonance wave function calculated in this way strongly depends on the initial wave function, and one must be careful for further studying with it.

Instead, a rigorous, robust, and convenient method to calculate the dynamical resonance wave functions in a reactive process may be applied, which is a direct extension of the standard TDWP method for describing a reaction scattering process. For a reactive scattering of a triatomic $A + BC$ reaction with the initial incoming wave function $\Psi^{JM\epsilon}_{v_0 j_0 l_0}(t=0)$ for an initial state (v_0, j_0, l_0), the dynamical resonance wave function at certain collision energy E_n can be obtained with a Fourier transform of the time evolved incoming wave function as

$$\Phi(E_n) = \sum_{l_0,\epsilon} \int_{-\infty}^{+\infty} \Psi^{JM\epsilon}_{v_0 j_0 l_0}(t) \exp(iE_n t) dt \equiv \sum_{l_0,\epsilon} \int_{0}^{+\infty} \Psi^{JM\epsilon}_{v_0 j_0 l_0}(t) \exp(iE_n t) dt \tag{4.32}$$

The last step is reached by using the fact that before time zero the incoming wave contributes nothing to the interaction region. Thus the calculated resonance wave function is rigorous in the whole grid region and can be safely used to analyze the reactive process. The dynamical resonance wave function must have relatively large amplitude in the interaction region and pure incoming and outgoing tails with relatively small amplitude, and exhibits features of a quasi-bound state. And we can use this evidence to justify if the calculated wave function at specified collision energies corresponds to a dynamic resonance state. In contrast to the spectral

quantization method, the wave function in resonance region may not be so clear since it is not overemphasized.

After the extraction of the reactive resonance wave function in certain convenient coordinates used in the propagation, one may need to transform it into another optimal coordinates to facilitate the observation of its resonance quantization structure, such as normal mode near the transition state region or product/reactant Jacobi coordinates or hyperspherical coordinates. In this way, the dynamics origin of the reactive resonance wave functions may be clarified to us.

4.4 Applications

4.4.1 Resonances in F Plus H_2 and Its Isotopes

The reactive resonances reveal the quasi-bound levels of the reaction complex with unique clarity and they do exist. Identification of the reactive resonances can help us with understanding how elementary chemical processes take place at a single quantum state level. $F + H_2$ and its isotopic analogs are the most beautiful examples.

Interest in the $F + H_2$ reaction was largely due to Lee's benchmark molecular beam studies [105] and early chemiluminescence and chemical laser work [98]. This work led to the early QCT studies of Muckerman [88], Blais and Truhlar [13], and Polanyi and Schreiber [97], using the PES but with serious flaws. A series of surface by Truhlar and his coworkers [17, 84, 122, 135] led to gradual improvement, and then Stark and Werner developed surfaces (SW PES) [121] from multireference configuration interaction calculations that resolved many of the earlier issues, even some problems remain. Very recently, Zhang and his coworkers developed several versions of the PES for the $F + H_2$ reaction using icMRCI [100] and CCSDT method [40, 102], whose ultimate version has been proved to be of spectroscopy accuracy.

Early the QCT [106] and collinear quantum reactive scattering studies [113] revealed their distinct difference for predicting the $F + H_2$ reaction, especially for the F + HD reaction where reactive resonances played a big role. Subsequent 3D quantum scattering calculations by Wyatt and coworkers [77, 78] and a variety of 3D quantum models confirmed the existence of the resonance, thereby stimulating further experiments on $F + H_2$ and its isotopic analogs and finally leading to the molecular beam studies of Neumark and coworkers [91–94] which proved important hints that resonances play a role in this reaction.

However, the following theoretical work on the SW PES argued that the forward scattering of the $F + H_2$ reaction results from the tunneling-induced reactivity at high impact parameters which do not need the formation of resonance [20]. And the QCT work by Aoiz et al. [9] yielded angular distributions with forward components that were consistent with the experiments, suggesting that the quantum effects, especially resonance effects, are relatively unimportant.

In 2000, the work on the F + HD reaction of Dong et al. [31] discovered the existence of reactive resonances in crossed beam experiments, where a

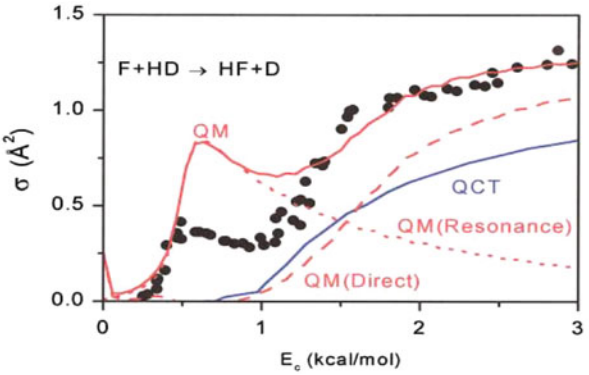

Fig. 4.4 The excitation functions for $F + HD \rightarrow HF + D$. The experimental results are shown with *solid dots*, the QCT simulations with a *blue line*, and the QM results with a *red line*. The resonance contribution is depicted with a *dotted red line*, and the direct reaction contribution with a *dashed red line*. A multisurface factor of 1/2 has been used to scale the ICS

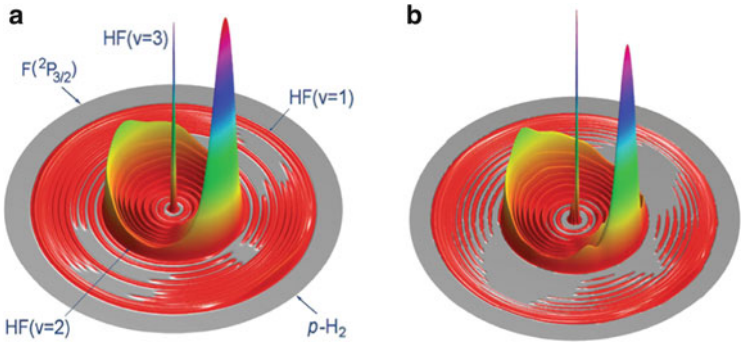

Fig. 4.5 Experimental (**a**) and theoretical (**b**) 3D contour plots for the product translational energy and angle distributions for the $F(^2P_{3/2}) + H_2(j_0 = 0)$ reaction at the collision energy of 0.52 kcal/mol. The *different circles* represent different HF product ro-vibrational states. The forward-scattering direction for HF is defined along the F atom beam direction

resonance-enhanced step in the excitation function was observed, as shown in Fig. 4.4. Subsequent IR work by Nesbitt [48] confirmed this results and theoretical calculations have been presented to interpret the dynamics using SW PES [116,117].

In 2006, the work of Qiu et al. [100] presented the evidence for the resonances in the $F + H_2$ reaction, with both theory and experiment exhibiting consistent behavior on XXZ PES, as shown in Fig. 4.5. The appearance of this report is catalyzed by the developments on quantum scattering method development, ab initio method and crossed-molecular beam combined with high resolution H-Rydberg state tagging technique [147]. The sharp forward peak at collision energy of 0.52 kcal/mol actually results from the interference between the first two Feshbach resonances. For total angular momentum $J = 0$, there are two resonance states at collision

energy of 0.26 and 0.46 kcal/mol. With increasing J, the resonance energy will shift to higher collision energy. The three-dimensional (3D) scattering wave function at the collision energy of 0.26 kcal/mol shows the existence of three nodes along the H-F coordinate (correlating to the HF product) in the HF-H′ complex with no node along the reaction coordinate. The projection of the $J = 0$ scattering wave function at 0.26 kcal/mol to the HF vibrational states shows that the main character in this wave function is HF($v' = 3$) with the outgoing waves mostly on HF($v' = 2$). This implies that the resonance state at 0.26 kcal/mol is the ground resonance state, (003), trapped in the HF($v' = 3$)-H′ vibrational adiabatic potential (VAP) well. The 3D scattering wave function for $J = 0$ at the collision energy of 0.46 kcal/mol shows the existence of three nodes along the HF coordinate (correlating to the HF product) in the HF-H′ complex with one node along the reaction coordinate. The projection of the $J = 0$ scattering wave function at 0.46 kcal/mol to the HF vibrational states shows the main character in this wave function is predominantly HF($v' = 3$) with the outgoing waves also mostly on HF($v' = 2$). This suggests that the resonance state at 0.46 kcal/mol is the excited reaction resonance state trapped in the HF($v' = 3$)-H′ VAP well. This resonance state can be assigned to the (103) resonance state with one-quantum vibration along the reaction coordinate, zero-quantum vibration on the bending motion (or hindered rotation), and three-quanta vibration along the HF stretching. The resonance schemes were shown in Fig. 4.6.

Their subsequent work at higher collision energy (0.94 kcal/mol) demonstrated the tunneling and shape resonance effects [139], other than Feschbash resonance for arising the forward scattering in the reaction of $F + H_2$, which suggested that the reactive resonances played quite different roles in the same reaction but at different collision energies [139].

In 2008, Ren et al. [102] measured the DCSs at several collision energies, which showed strong variation as a function of collision energies, as shown in Fig. 4.7, due to the existence of strong reactive resonance state. The theoretical DCSs on the new version PES by Zhang and his coworkers (FXZ PES) agree with the experimental observation very well, as shown in Fig. 4.8 which demonstrated that the $F + H_2$ reaction is the first reaction which can be studied at spectroscopy accuracy, besides the $H + H_2$ reaction.

To have a better feeling about the resonance state, the ground reactive resonance state wave function of the $F + HD \rightarrow HF + D$, along with the 2D minimal potential, which is optimized along the angle degree of freedom, is given in Fig. 4.9. It is observed there that the wave function exhibits well features of a semi-bound state. The outgoing part, which corresponds to the HF ($v' = 2$) product, has two nodes of structure but the inside peak has three nodes, which corresponds to an excited vibrational state of $v' = 3$.

The most exciting chapter on detecting the reactive resonances in the $F + H_2$ reaction and its isotopic analogs is the observation of the partial wave resonance in the F + HD by Dong et al. in 2010 [32]. The reactive resonance, as we know, which commonly is considered as being elusive and smeared by summation of many partial waves, was observed individually by Dong et al. at three different rotational quantum states of the temporarily trapped FHD complex, as shown in Fig. 4.10.

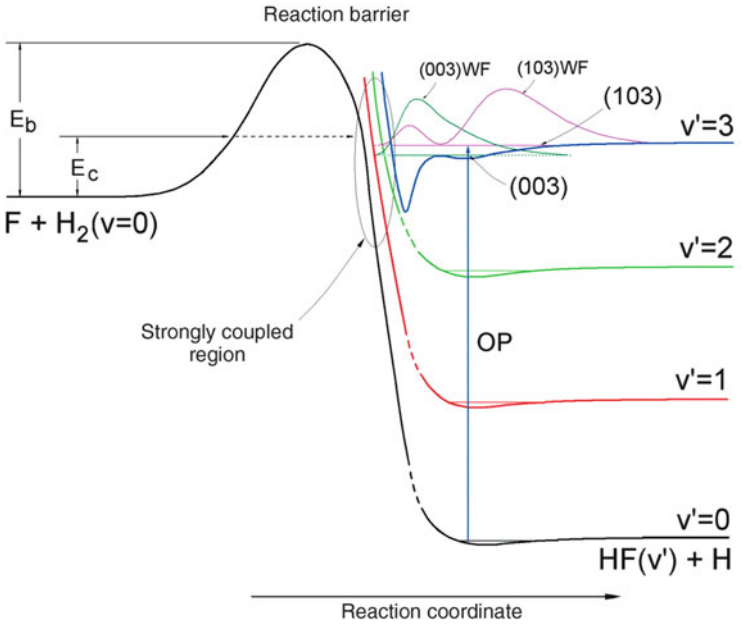

Fig. 4.6 Schematic diagram showing the resonance-mediated reaction mechanism for the $F + H_2$ reaction with two resonance states trapped in the peculiar HF($v' = 3$)-H′ VAP well. The 1D wave functions of the two resonance states are also shown. The (003) state is the ground resonance state; the (103) resonance is the first excited resonance state. Calculated van der Waals states for the lower VAPs are also shown. OP, overtone pumping; E_b, barrier height; E_c, collision energy

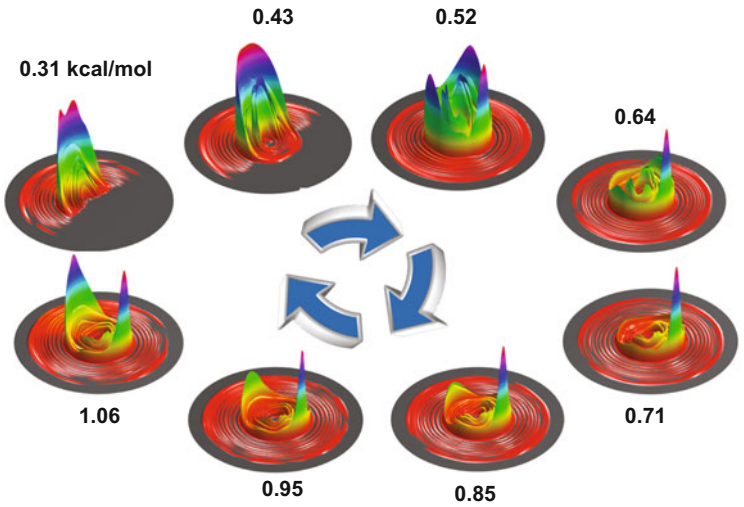

Fig. 4.7 The experimental 3D contour plots for the product translational energy and angular distributions for the $F(^2P_{3/2}) + HD(j_0 = 0)$ reaction at various collision energies: 0.31, 0.43, 0.52, 0.64, 0.71, 0.85, 0.95, and 1.06 kcal/mol

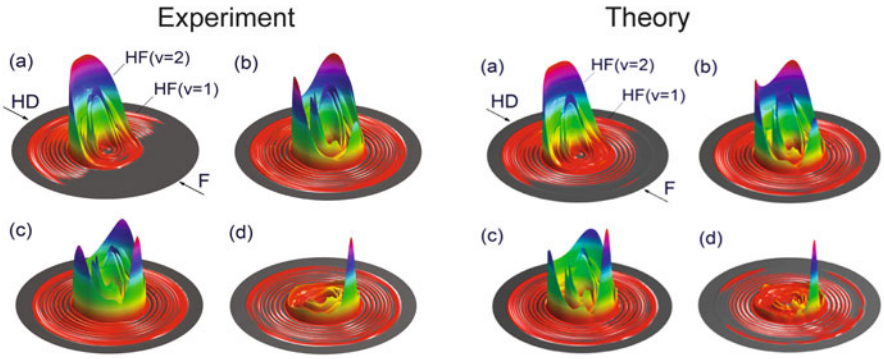

Fig. 4.8 The experimental and theoretical 3D contour plots for the product translational energy and angular distributions for the $F(^2P_{3/2}) + HD(j_0 = 0)$ reaction at various collision energies: 0.43 kcal/mol (**a**); 0.48 kcal/mol (**b**); 0.52 kcal/mol (**c**); and 0.71 kcal/mol (**d**)

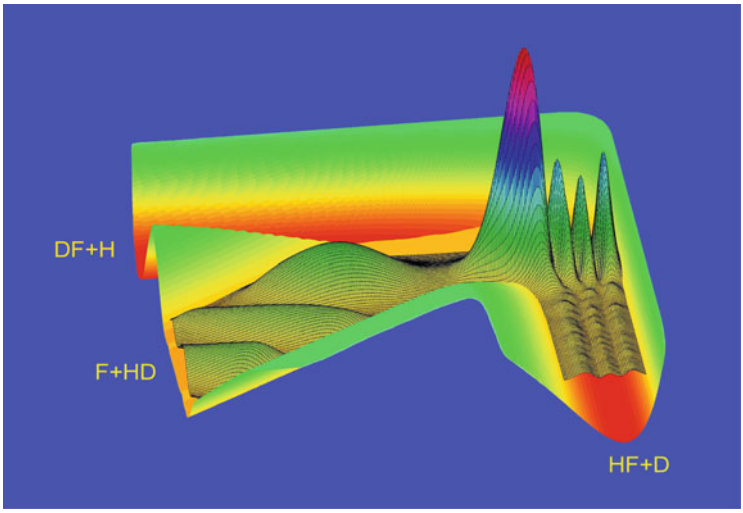

Fig. 4.9 3D ground reactive resonance wave function of the $F + HD$ ($v_0 = 0$, $j_0 = 0$) $\rightarrow HF + D$ reaction, along with the potential which is optimized along angle degree of freedom

This is different from the work in 2000 by Dong et al. [31] where the resonance in $F + HD$ was identified by observing the averaged contribution from a sequence of the resonances in the cross sections. Dong et al. are, however, in 2010 the first to pick out individual resonances from this series [32].

Recent quantum reactive scattering studies of $F + H_2$ and $Cl + H_2$ have included spin-orbit effects and multiple surfaces within both the framework of hyperspherical coordinate coupled channel and TDWP calculations [2, 129, 140]. These works help us with better understanding the role of the spin-orbit effects in reactions.

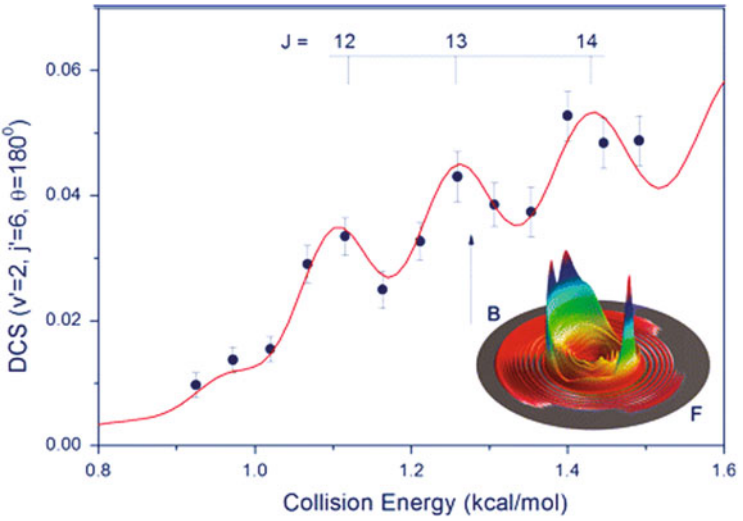

Fig. 4.10 Experimental and theoretical DCS of the HF($v = 2$, $j = 6$) product of the $F(^2P_{3/2}) + HD(j_0 = 0)$ reaction in the backward scattering direction. The *solid circles* are experimental data; the *red curve*, the result of full quantum dynamics calculations convoluted with the experimental resolution and shifted 0.03 kcal/mol lower in energy. The error bars in the experimental data are the estimated measurement errors (1σ) for the HF($v = 2$, $j = 6$) product peak intensity in the collision energy scan. The three peaks are assigned to the partial wave Feshbach resonances of $J = 12$, 13, and 14 in the $F + HD \rightarrow HF + D$ reaction, as explained in the text. The three-dimensional DCS shown was measured at 1.285 kcal/mol, with F and B indicating the forward- and backward-scattering, respectively, directions for HF with respect to the F-atom beam direction

From above discussion, we have seen a close interplay between theory and experiment which is extremely helpful with revealing the reaction dynamics mechanism. Theory and experiment verify and reinforce each other, develop side by side through mutual cross-fertilization. We can expect even more success through a close interplay between them.

4.4.2 Non-statistical Effects in $H + O_2$ Reaction

The $H + O_2 \rightarrow HO + O$ reaction and its reverse are of fundamental importance to combustion chemistry. This reaction proceeds via the formation of an intermediate complex in a deep well of 2.4 eV which is relatively stable with no barrier to dissociation. There have been many theoretical and experimental studies on this reaction, particularly on the concern about the non-statistical effects. Statistical modeling based on the statistical adiabatic channel model (SCAM) is able to account for the observed forward and reverse thermal rate constants overall a wide range of temperature, implying that the reaction is statistical. However, QCT studies find

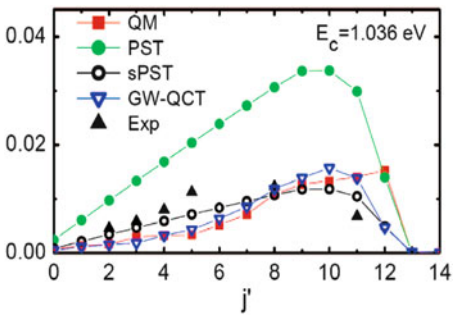

Fig. 4.11 Comparison of the QM rotational state distribution of OH (*filled square*) with the PST results (*filled circle*), GW-QCT results (*filled inverted triangle*), and available experimental data (*filled triangle*). The PST result normalized to the QM distribution (sPST) is also presented (*open circle*)

that there is significant recrossing of reasonably chosen dividing surfaces after the HO_2 complex is formed in the $HO + O$ reaction, suggesting the existence of the important non-statistical effects in this reaction. Rigorous quantum reactive scattering calculations and more accurate potentials are required to settle down this issue. However, this reaction presents obvious challenges for quantum scattering calculations, on account of the heavy masses and the deep HO_2 well.

Using DMBE IV potential, Meijer and coworkers carried out wavepacket calculations of the initial state selected total cross sections for the $H + O_2$, including partial waves up to $J = 35$. All of the projections of J onto the intermolecular axis have been incorporated in the calculations. They found that the calculated cross sections are lower than the experiment, which indicated the deficiencies in the DMBE IV potentials. In 2005, Xu et al. constructed a new potential (XXZLG PES) for this reaction at the internally contracted multireference configuration interaction plus the Davidson correction level with the augmented correlation consistent polarized valence quadruple zeta (aug-cc-pVQZ) basis set. It has been shown that there is remarkable improvement over the previous DMBE IV potential. Based upon this new potential and using the recent developed RCB quantum wave packet method, Sun et al. calculated state-to-state DCS and ICS of the $H + O_2$ reaction up to 1.5 eV.

By comparing the QM rotational state distribution with the statistical limit represented by the phase space theory (PST), which assumes that the formation and decay of the reaction intermediate are separate events and the decay probability is proportional to the number of open channels. As shown in Fig. 4.11, the shape of the PST distribution is similar to that of the QM counterpart; namely, it increases with j until the highest accessible rotational state. However, the statistical model severely overestimates the QM distribution. Even when comparing with the normalized PST distribution, as shown in the same figure, the QM distribution typically overpopulates at large j values and underpopulates at small j values. Similar differences exist in other collision energies.

The deviation of the QM rotational state distribution from the statistical limit is a convincing piece of evidence in support of the argument that the title reaction has a significant non-statistical component despite its complex-forming nature. In other words, the dynamics plays a non-negligible role in the reaction. This is contrast with

the conventional wisdom: usually it is assumed that the deep well in the PES which creates the long-lifetime intermediate complex will smear out all of the dynamics effect thus leads to statistical limit. This conclusion is consistent with the slight forward–backward asymmetry of the calculated DCSs reported here and the non-statistical decay of the HO_2 complex observed in QCT studies. The origin of the non-statistical behavior can presumably be attributed to the relatively short lifetime of the HO_2 intermediate which has not enough time to fully relax the internal energy into all degrees of the freedom in a statistical way.

The atmospherically important reaction $O + O_2$ with three heavy atoms and deep potential well has also been studied at the state-to-state DCS level by quantum wave packet method. It reveals the failure of the statisical model from the calculated strong non-statistical effects and some quantum effects in the reaction [128].

4.4.3 $H_2 + OH$

The $H_2 + OH \rightarrow H + H_2O$ reaction is a prototype reaction for H atom abstraction by an OH radical to form water as a product. Moreover, it is important in combustion chemistry and interstellar chemistry [85, 142]. Consequently, it has attracted extensive experimental and theoretical studies. Crossed-molecular beam experiments on the isotopically substituted $D_2 + OH \rightarrow D + HOD$ reaction revealed that the product was strongly backward-scattered, with the majority of the available energy channeled into HOD internal excitation and the newly formed OD bond in the HOD molecule preferentially excited to the $v = 2$ state [123]. The reverse reaction has also been studied widely as a prototype system for mode specific chemistry, in which different vibrational modes in the reactants can play an important role in the reaction dynamic. As three of the four atoms in this system are hydrogen isotopes, it has been straightforward to pursue both high-quality ab initio calculation of a PES and accurate quantum dynamics calculations. As a result, this reaction has become a benchmark system for four-atom reactions, in much the same role that the $H + H_2$ reaction played for three-atom reactions.

In 1993, the first TDWP calculation was reported for the $H_2 + OH \rightarrow H_2O + H$ reaction with the total angular momentum $J = 0$ by using diatom–diatom Jacobi coordinates with only the spectator OH bond length frozen [158]. It was quickly extended to include all degrees of freedom for a four-atom reaction without any dynamical approximate on the same reaction system [159]. In 1996, the TDWP method was applied to study the $H + H_2O \rightarrow H_2 + OH$ reaction in full dimensions on the atom–triatom Jacobi coordinates [161]. Then, the method was extended to study four-atom reactions for the total angular momentum $J > 0$ in one set of Jacobi coordinates, with the full converged integral cross sections reported for the $H_2 + OH \rightarrow H_2O + H$ reaction [155] in 1999, for the $H + D_2O \rightarrow D + HOD$ and $H_2O + H \rightarrow H_2 + OH$ reactions in 2000 [162, 164].

Figure 4.12 compares theoretical integral cross sections for the $H + D_2O \rightarrow D + HOD$ exchange reaction with the experimental results [18,19,162]: the absolute cross sections at a relative translational energy of 1.5 and 2.2 eV and the excitation

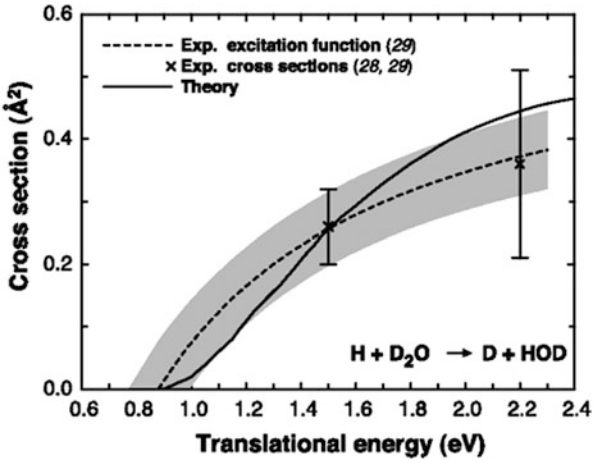

Fig. 4.12 Comparison between the experimental and theoretical integral cross sections for the $H + D_2O \rightarrow D + HOD$ reaction. The *dashed line* is the experimental excitation function. The *shaded area* reflects the statistical uncertainty (1σ) of the global least squares fit procedure used to determine the optimum excitation function

function of the reaction in the line-of-center functional model. The first-principles theoretical results agree excellently with the experiments in all respects. We note that the experimental result is thermally averaged over the initial rotation of D_2O, whereas the theoretical result is for initial non-rotating D_2O (preliminary calculations showed that rotational excitation of the triatomic reactant has no substantial effect on the integral cross section).

Despite the significant progress in initial state selected level, the accurate quantum calculation of the state-to-state DCSs for four-atom reactions remained a challenge for many years. State-to-state reaction probabilities for the total angular momentum $J = 0$ were reported for the $H_2 + OH \rightarrow H_2O + H$ reaction by using both the diatom–diatom and atom–triatom Jacobi coordinates [165]. Following that, the state-to-state integral and DCSs were reported for the $H + H_2O \rightarrow H_2 + OH$ reaction in five dimensions with the spectator OH bond length fixed, in 2002 [163] and 2005 [154], respectively. In the past few years, Althorpe and coworkers used quantum wave packet method to obtain the state-to-state reaction probability for the $H_2 + OH \rightarrow H_2O + H$ reaction in five and fully six dimensions [27–29]. All of these state-to-state calculations were using the reduced dimensionality method or limited to total angular momentum $J = 0$.

Recently, TDWP method was developed to compute DCSs for four-atom reactions and applied to the prototypical $HD + OH \rightarrow H_2O + D$ [70, 145] and $D_2 + OH \rightarrow HOD + D$ reactions [69]. Excellent agreements were achieved for the first time for a four-atom reaction between the full-dimensional DCS and high-resolution crossed-molecular beam experimental results on the $HD + OH \rightarrow H_2O + D$ reaction [145]. Figure 4.13 compares the theoretical energy

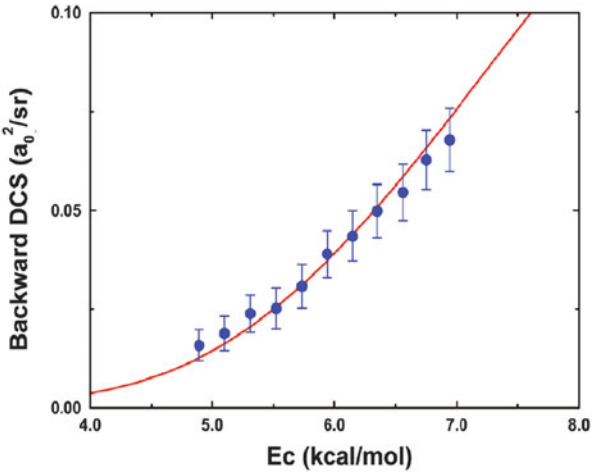

Fig. 4.13 Experimental and theoretical DCSs of the $HD + OH \rightarrow H_2O + D$ reaction in the backward scattering direction. The experimental data, measured in relative values, are scaled to the theoretical DCS value at the collision energy (E_c) of 6.15 kcal/mol. In the experiment, the DCSs at the backward scattering direction were measured by scanning the collision energy back and forth 15 times. Error bars in the experimental data indicate the estimated errors ($\pm 1\sigma$) for the DCS signal at the backward direction from the 15 scans of the collision energy

dependence of DCSs in the backward direction with the experimental result. The agreement between theory and experiment is remarkable. It also reveals that the theoretical reaction barrier of 5.4 kcal/mol on the PES they used is very accurate, and the quantum tunneling effect for the hydrogen transfer reaction is quite strong, since the reaction threshold is apparently much lower than the barrier height 5.4 kcal/mol.

4.4.4 OH + CO

After simple four-atom reactions have been solved, however, huge challenges still persist in rigorous quantum scattering studies of complex-forming four-atom reactions with more than one heavy atoms, such as the $OH + CO \rightarrow H + CO_2$. Because of its crucial role in the conversion of CO to CO_2, the $OH + CO \rightarrow H + CO_2$ reaction is important to both atmospheric [39] and combustion chemistry [86]. Due to the presence of two deep wells along the reaction path which support long-lived collision complex HOCO in both *trans* and *cis* configurations, the reaction dominated by pronounced resonances has become a prototype recently for complex-forming four-atom reactions, just as $H_2 + OH \rightarrow H + H_2O$ is for direct four-atom reactions.

Considerable experimental studies have been carried out on this reaction and its reverse [1, 61, 103]. Theoretically, in 1987 the first global analytic PES was constructed by Schatz, Fitzcharles, and Harding (denoted as SFH) based on the

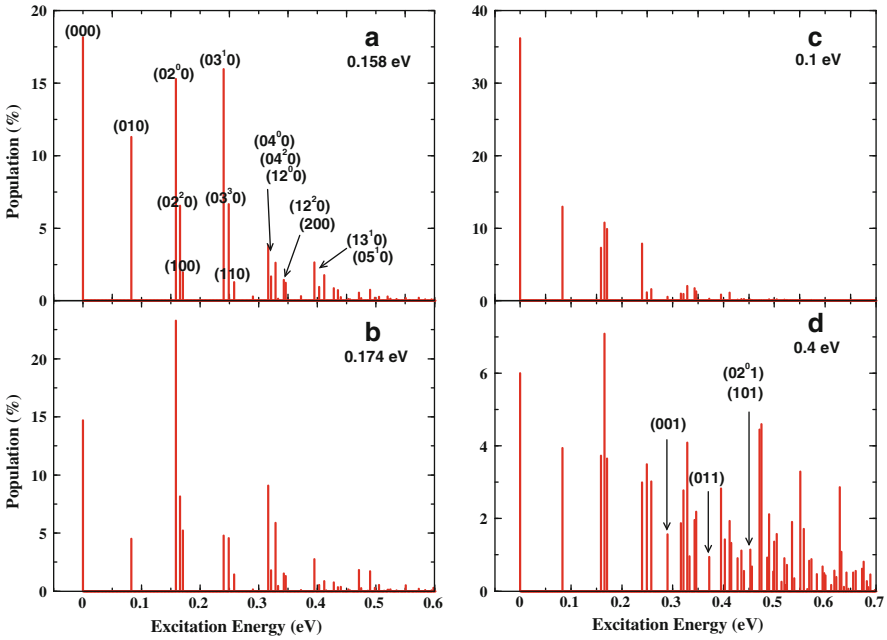

Fig. 4.14 Product vibrational state distributions of CO_2 for the $OH + CO \rightarrow H + CO_2$ reaction with total angular momentum $J = 0$ at reactant translational energy of (**a**) 0.158 eV, (**b**) 0.174 eV, (**c**) 0.1 eV, and (**d**) 0.4 eV

many-body expansion approach [114]. Following that, a number of global analytic [58,59,150] and numerical [25,63] PES have been constructed to study the reaction more accurately, and many dynamics calculations have been performed by using quasiclassical trajectory method [59, 79]. We would like to note here that there is more detailed discussion about this reaction in the chapter by Guo et al. in this book.

The $OH + CO$ reaction presents a huge challenge to quantum dynamics. The combination of a relatively long-lived collision complex and three heavy atoms in this reaction makes the rigorous quantum scattering calculations difficult. Kroes and coworkers obtained the first 6D total reaction probabilities for this reaction. Very large basis sets had to be used to ensure converged results [138]. Recently, Zhang and coworkers gave some preliminary full-dimensional (6D) quantum state-to-state results for this reaction on the LTSH PES. It is the first such a calculation for a four-atom reaction other than the $H_2 + OH \leftrightarrow H_2O + H$ and its isotopically substituted reactions. The calculation is carried out by the RPD method. The results presented are limited to total angular momentum $J = 0$ for the ground initial ro-vibrational state. Advancing from $J = 0$ to $J > 0$ is extremely difficult due to the rapid increase of the rotational basis functions needed in calculation [68].

Figure 4.14 shows the CO_2 product vibrational state distributions at four collision energies. For CO_2, because the symmetric stretching vibrational frequency ν_1 is

very close to the double of the bending frequency ν_2, it is extremely hard to make a complete assignment of all the vibrational states, and they only managed to assign some of the vibrational states with low excitation energies. The total reaction probability exhibits a pronounced peak at $E_c = 0.158\,\text{eV}$ and a dip at $E_c = 0.174\,\text{eV}$. Although the total and, therefore the CO_2 vibrational state-specific reaction probabilities at 0.158 eV are much larger than at 0.174 eV, the population structures for the two collision energies are quite similar. The (000) state has large population, but the majority of the population are contributed by the bending excited states. Figure 4.3c, d present the CO_2 vibrational population at $E_c = 0.1$ and 0.4 eV, to show the effect of collision energy on product vibrational state distribution.

4.5 Conclusion

After persistent endeavors of decades, the quantum wave packet method has been well developed and currently it is quite mature for calculating product state-resolved different cross sections of triatomic and tetra-atomic reactive scatterings. However, due to numerical scaling of a quantum calculation, in order to study more complicated systems, developments of more efficient numerical methods are still very important in the future, such as the search and develop more efficient grid representation for angular degree of freedom and more compact Hamiltonian forms etc.

MCTDH method has been proven being efficient and memory-saving for dealing with polyatomic molecular dynamics. Theoretical methods for approximately extracting state-to-state differential cross section using MCTDH method would be worth more investigating, particularly for the reaction $H + CH_4$ and its isotopic analogs.

Resonances in triatomic reactive scattering from the reactants in ground vibrational state have been identified and characterized, which help us to deepen the understanding of the chemical reaction dynamics at a single quantum state level. Reactive resonances in a polyatomic reaction and reaction starting with initial states other than ground vibrational states will receive more interest, along with the experimental techniques development [141]. This in turn stimulates the theoretical endeavors for more efficient theoretical methods. In a cold chemical reaction, similar resonance would, in principle, easier to be experimentally observed since there are only very limited partial waves involved. The techniques developed in this chapter can be applied to study the resonance in a cold chemical reaction straightforward.

Acknowledgments We acknowledge X.M. Yang (DICP), H. Guo (UNM), D.Q. Xie (NJU), M. Alexander (UM), Soo-Y. Lee for helpful discussion and cooperated work. Funding supports from Chinese Academy of Sciences and NSFS (Grant No. 21222308, 21103187, 21133006) are acknowledged.

References

1. Alagia M, Casavecchia P, Stranges D (1993) Crossed beam studies of four-atom reactions: the dynamics of OH + CO. J Chem Phys 98:8341
2. Alexander MH, Manolopoulos DE, Werner HJ (2000) An investigation of the F + H_2 reaction based on a full ab initio description of the open-shell character of the F(^2P) atom. J Chem Phys 113(24):11084
3. Althorpe SC (2001) Quantum wavepacket method for state-to-state reactive cross sections. J Chem Phys 114(4):1601
4. Althorpe SC, Clary DC (2003) Quantum scattering calculations on chemical reactions. Annu Rev Phys Chem 54:493
5. Althorpe S, Kouri D, Hoffman D (1997) A chebyshev method for calculating state-to-state reaction probabilities from the time-independent wavepacket reactant-product decoupling equations. J Chem Phys 106:7629
6. Althorpe SC, Kouri DJ, Hoffman DK (1997) Further partitioning of the reactant-product decoupling equations of state-to-state reactive scattering and their solution by the time-independent wave-packet method. J Chem Phys 107(19):7816
7. Althorpe SC, Kouri DJ, Hoffman DK, Zhang JZH (1997) Reactantproduct decoupling approach to state-resolved reactive scattering time-independent wavepacket formulation. J Chem Soc Faraday Trans 93(5):703
8. Althorpe S, Fernández-Alonso F, Bean B, Ayers J, Pomerantz A, Zare R, Wrede E (2002) Observation and interpretation of a time-delayed mechanism in the hydrogen exchange reaction. Nature 416:67
9. Aoiz FJ, Bañares L, Martinez-Haya B, Castillo JF, Manolopoulos DE, Stark K, Werner HJ (1997) Ab initio simulation of molecular beam experiments for the F + H_2 → HF + H reaction. J Phys Chem A 101(36):6403
10. Askar A, Cakmak AS (1978) Explicit integration method for the time-dependent Schrödinger equation for collision problems. J Chem Phys 68:2794
11. Bandrauk AD, Shen H (1991) Improved exponential split operator method for solving the time-dependent Schrödinger equation. Chem Phys Lett 176:428
12. Beck MH, Jäckle A, Worth GA, Meyer HD (2000) The multiconfiguration time-dependent Hartree method: a highly efficient algorithm for propagating wavepackets. Phys Rep 324:1
13. Blais NC, Truhlar DG (1973) Monte carlo trajectories: dynamics of the reaction F + D_2 on a semiempirical valencebond potential energy surface. J Chem Phys 58(3):1090
14. Blanes S, Casas F, Murua A (2006) Symplectic splitting operator methods for the time-dependent Schrödinger equation. J Chem Phys 124:234105
15. Bowman JM, Schatz GC (1995) Theoretical studies of polyatomic bimolecular reaction dynamics. Annu Rev Phys Chem 46(1):169
16. Brink DM, Satchler GR (1968) Angular momentum. Clarendon, Oxford
17. Brown FB, Steckler R, Schwenke DW, Truhlar DG, Garrett BC (1985) An improved potential energy surface for F + H_2 → HF + H and H + HFHF + H. J Chem Phys 82(1):188
18. Brownsword R, Hillenkamp M, Laurent T, Vatsa RK, Volpp HR, Wolfrum J (1996) Dynamics of the H + D_2O → D + HOD hydrogen exchange reaction. Chem Phys Lett 259:375
19. Brownsword R, Hillenkamp M, Laurent T, Vatsa RK, Volpp HR, Wolfrum J (1997) Excitation function and reaction threshold studies of isotope exchange reactions: H + D_2 → D + HD and H + D_2O → D + HOD. J Phys Chem A 101:6448
20. Castillo JF, Manolopoulos DE, Stark K, Werner HJ (1996) Quantum mechanical angular distributions for the F + H_2 reaction. J Chem Phys 104(17):6531
21. Cerjan C (ed) (1993) Numerical grid methods and their application to Schrödinger's equation. Springer, New York
22. Chao SD, Skodje RT (2002) Signatures of reactive resonance: three case studies. Theor Chem Acc 108(5):273

23. Chatfield DC, Friedman RS, Schwenke DW, Truhlar DG (1992) Control of chemical reactivity by quantized transition states. J Phys Chem 96(6):2414
24. Chen R, Guo H (1999) The chebyshev propagator for quantum systems. Comput Phys Commun 119(1):19
25. Chen J, Xu X, Zhang D (2013) An accurate global potential energy surface for the OH + CO → H + CO_2 reaction using neural networks. J Chem Phys 138:221104
26. Clary DC (1994) 4-Atom reaction dynamics. J Phys Chem 98:10678
27. Cvitas M, Althorpe S (2009) Quantum wave packet method for state-to-state reactive scattering calculations on AB + CD → ABC + D reactions. J Chem Phys 113:4557
28. Cvitas M, Althorpe S (2009) State-to-state reactive scattering using reactant-product decoupling. Phys Scr 80:048115
29. Cvitas M, Althorpe S (2011) State-to-state reactive scattering in six dimensions using reactant-product decoupling: OH + H_2 → H_2O + H ($J = 0$). J Chem Phys 134:024309
30. Dai J, Zhang JZH (1996) Time-dependent wave packet approach to state-to-state reactive scattering and application to h + o2reaction. J Phys Chem 100(17):6898
31. Dong F, Lee SH, Liu K (2000) Reactive excitation functions for F + p-H_2/n-H_2/D_2 and the vibrational branching for F + HD. J Chem Phys 112(9):3633
32. Dong W, Xiao C, Wang T, Dai D, Yang X, Zhang DH (2010) Transition-state spectroscopy of partial wave resonances in the f + hd reaction. Science 327(5972):1501
33. Evans MG (1938) Thermodynamical treatment of transition state. Trans Faraday Soc 34:49
34. Evans MG, Polanyi M (1935) Some applications of the transition state method to the calculation of reaction velocities, especially in solution. Trans Faraday Soc 31(1):0875
35. Eyring H (1935) The activated complex in chemical reactions. J Chem Phys 3(2):107
36. Feit MD, Fleck JA Jr, Steiger A (1982) Solution of the Schrödinger-equation by a spectral method. J Comput Phys 47:412
37. Fernandez-Alonso F, Zare RN (2002) Scattering resonances in the simplest chemical reaction. Annu Rev Phys Chem 53:67
38. Fernández-Ramos A, Miller JA, Klippenstein SJ, Truhlar GD (2006) Modeling the kinetics of bimolecular reactions. Chem Rev 106:4518
39. Finlayson-Pitts B, Pitts J (2000) Chemistry of the upper and lower atmosphere. Academic, London
40. Fu B, Xu X, Zhang DH (2008) A hierarchical construction scheme for accurate potential energy surface generation: an application to the F + H_2 reaction. J Chem Phys 129(1):011103
41. Gogtas F, Balint-Kurti GG, Offer AR (1996) Quantum mechanical three-dimensional wavepacket study of the Li + HFLiF + H reaction. J Chem Phys 104(20):7927
42. Goldfield E, Gray S (2002) A quantum dynamics study of H_2 + OH → H_2O + H employing the Wu–Schatz–Lendvay–Fang–Harding potential function and a four-atom implementation of the real wave packet method. J Chem Phys 117:1604
43. Gomez-Carrasco S, Roncero O (2006) Coordinate transformation methods to calculate state-to-state reaction probabilities with wave packet treatments. J Chem Phys 125(5):054102
44. Gray SK, Balint-Kurti GG (1998) Quantum dynamics with real wave packets, including application to three-dimensional (j = 0)d + h[sub 2]hd + h reactive scattering. J Chem Phys 108(3):950
45. Gray SK, Manolopoulos DE (1996) Symplectic integrators tailored to the time-dependent Schrödinger equation. J Chem Phys 104:7099
46. Guo H (2012) Quantum dynamics of complex-forming bimolecular reactions. Int Rev Phys Chem 31(1):1
47. Hankel M, Balint-Kurti GG, Gray SK (2000) Quantum mechanical calculation of product state distributions for the o([sup 1]d) + h[sub 2]oh + h reaction on the ground electronic state surface. J Chem Phys 113(21):9658
48. Harper WW, Nizkorodov SA, Nesbitt DJ (2002) Reactive scattering of F + HD → HF(v, J) + D:HF(v, J) nascent product state distributions and evidence for quantum transition state resonances. J Chem Phys 116(13):5622

49. Hirschfelder J, Eyring H, Topley B (1936) Reactions involving hydrogen molecules and atoms. J Chem Phys 4(3):170
50. Hu W, Schatz GC (2006) Theories of reactive scattering. J Chem Phys 125(13):132301
51. Huang Y, Kouri DJ, Hoffman DK (1994) General, energy-separable Faber polynomial representation of operator functions: theory and application in quantum scattering. J Chem Phys 101:10493
52. Hulburt HM, Hirschfelder JO (1943) The transmission coefficient in the theory of absolute reaction rates. J Chem Phys 11(6):276
53. Judson R, Kouri D, Neuhauser D, Baer M (1990) Time-dependent wave-packet method for the complete determination of s-matrix elements for reactive molecular collisions in three dimensions. Phys Rev A 42(1):351
54. Karplus M, Porter RN, Sharma RD (1965) Exchange reactions with activation energy. i. simple barrier potential for (h, h2). J Chem Phys 43(9):3259
55. Kosloff R (1994) Propagation methods for quantum molecular dynamics. Ann Rev Phys Chem 45:145
56. Kosloff D, Kosloff R (1983) A Fourier method solution for the time dependent Schrödinger equation: a study of the reaction $H^+ + H_2$, $D^+ + HD$, and $D^+ + H_2$. J Chem Phys 79:1823
57. Kosloff D, Kosloff R (1983) A Fourier method solution for the time dependent Schrödinger equation as a tool in molecular dynamics. J Comput Phys 52:35
58. Kudla K, Schatz G, Wagner A, Harding L (1991) A quasiclassical trajectory study of the OH + CO reaction. J Chem Phys 95:1635
59. Lakin M, Troya D, Schatz G, Harding L (2003) A quasiclassical trajectory study of the reaction $OH + CO \rightarrow H + CO_2$. J Chem Phys 119:5848
60. Leforestier C, Bisseling RH, Cerjan C, Feit MD, Friesner R, Guldenberg A, Hammerich A, Jolicard G, Karrlein W, Meyer HD, Lipkin N, Roncero O, Kosloff R (1991) A comparison of different propagation schemes for the time dependent Schrödinger equation. J Comput Phys 94:59
61. Lester M, Pond B, Anderson D (2000) Exploring the oh + co reaction coordinate via infrared spectroscopy of the OH–CO reactant complex. J Chem Phys 113:9889
62. Levine RD, Wu SF (1971) Resonances in reactive collisions: computational study of the h + h2 collision. Chem Phys Lett 11(5):557
63. Li J, Wang Y, Jiang B, Ma J, Dawes R, Xie D, Bowman J, Guo H (2012) A chemically accurate global potential energy surface for the ho + co $\rightarrow$ h + co_2 reaction. J Chem Phys 136:041103
64. Light JC, Carrington T (2000) Discrete-variable representations and their utilization. Adv Chem Phys 114:263
65. Lin S, Guo H (2006) Quantum state-to-state cross sections for atom-diatom reactions: a chebyshev real wave-packet approach. Phys Rev A 74(2):022703
66. Liu K (2001) Crossed-beam studies of neutral reactions: state-specific differential cross sections. Annu Rev Phys Chem 52:139
67. Liu K (2012) Quantum dynamical resonances in chemical reactions: from a + bc to polyatomic systems. Adv Chem Phys 149:1
68. Liu S, Xu X, Zhang D (2011) State-to-state quantum dynamics study of the $OH + CO \rightarrow H + CO_2$ reaction in full dimensions ($J = 0$). J Chem Phys 135:141108
69. Liu S, Xiao C, Wang T, Xu X, Zhang D, Yang X (2012) The dynamics of the $D_2 + OH \rightarrow HOD + D$ reaction: a combined theoretical and experiment study. Faraday Discuss 157:101
70. Liu S, Xu X, Zhang D (2012) Time-dependent wave packet theory for state-to-state differential cross sections of four-atom reactions in full dimensions: application to the $HD + OH \rightarrow H_2O + D$ reaction. J Chem Phys 136:144302
71. Liu S, Chen J, Zhang Z, Zhang D (2013) A six-dimensional state-to-state quantum dynamics study of the $H + CH_4 \rightarrow H_2 + CH_3$ reaction ($j = 0$). J Chem Phys 138:011101
72. Manthe U, Matzkies F (2000) Rotational effects in the $H_2 + OH \rightarrow H_2O + H$ reaction rate: full-dimensional close-coupling results. J Chem Phys 113:5725

73. Manthe U, Meyer HD, Cederbaum LS (1992) Wave-packet dynamics within the multiconfiguration Hartree framework: general aspects and application to NOCl. J Chem Phys 97:3199–3213
74. Manz J (1996) Molecular wavepacket dynamics: thoery for experiments 1926–1996. In: Nobel symposium book: femtochemistry and femtobiology. Imperial College Press, London
75. Marcus RA (1966) On the analytical mechanics of chemical reactions. Classical mechanics of linear collisions. J Chem Phys 45(12):4500
76. Marcus RA (1966) On the analytical mechanics of chemical reactions. Quantum mechanics of linear collisions. J Chem Phys 45(12):4493
77. McNutt JF, Wyatt RE, Redmon MJ (1984) Quantum dynamics of the threedimensional $F + H_2$ reaction. I. Energy partitioning and entropy analysis in the collision complex. J Chem Phys 81(4):1692
78. McNutt JF, Wyatt RE, Redmon MJ (1984) Quantum dynamics of the threedimensional $F + H_2$ reaction. II. Scattering wave function density and flux analysis. J Chem Phys 81(4):1704
79. Medvedev D, Gray S, Goldfield E, Lakin M, Troya D, Schatz G (2004) Quantum wave packe and quasiclassical trajectory studies of OH + CO: influence of the reactant channel well on thermal rate constants. J Chem Phys 120:1231
80. Meijer AJHM, Goldfield EM (1998) Time-dependent quantum mechanical calculations on h + o[sub 2] for total angular momentum j>0. J Chem Phys 108(13):5404
81. Meyer HD, Worth GA (2003) Quantum molecular dynamics: propagating wavepackets and density operators using the multiconfiguration time-dependent Hartree (MCTDH) method. Theor Chem Acc 109:251–267
82. Meyer HD, Manthe U, Cederbaum LS (1990) The multi-configurational time-dependent Hartree approach. Chem Phys Lett 165:73–78
83. Meyer HD, Gatti F, Worth GA (eds) (2009) Multidimensional quantum dynamics, 1st edn. Wiley, London
84. Mielke SL, Lynch GC, Truhlar DG, Schwenke DW (1993) A more accurate potential energy surface and quantum mechanical cross section calculations for the $F + H_2$ reaction. Chem Phys Lett 213(1):10
85. Millar T, Williams D (1988) Rate coefficients in atmospheric chemistry. Kluwer, Dordrecht
86. Miller J, Kee R, Westbrook C (1990) Chemical kinetics and combustion modeling. Annu Rev Phys Chem 41:345
87. Mowrey RC, Kouri DJ (1986) Closecoupling wave packet approach to numerically exact moleculesurface scattering calculations. J Chem Phys 84:6466
88. Muckerman JT (1971) Monte carlo calculations of energy partitioning and isotope effects in reactions of fluorine atoms with H_2, HD, and D_2. J Chem Phys 54(3):1155
89. Neuhauser D, Baer M, Judson RS, Kouri DJ (1990) A time-dependent wave packet approach to atomdiatom reactive collision probabilities: theory and application to the $H + H_2$ ($J = 0$) system. J Chem Phys 93(1):312
90. Neuhauser D, Baer M, Judson RS, Kouri DJ (1991) The application of time-dependent wavepacket methods to reactive scattering. Comput Phys Commun 63(13):460
91. Neumark D, Wodtke A, Robinson G, Hayden C, Lee Y (1984) Experimental investigation of resonances in reactive scattering: the $F + H_2$ reaction. Phys Rev Lett 53(3):226
92. Neumark DE, Wodtke AM, Robinson GN, Hayden CC, Lee YT (1984) Dynamic resonances in the reaction of fluorine atoms with hydrogen molecules. ACS Symp Ser 263:479
93. Neumark DM, Wodtke AM, Robinson GN, Hayden CC, Lee YT (1985) Molecular beam studies of the $F + H_2$ reaction. J Chem Phys 82(7):3045
94. Neumark DM, Wodtke AM, Robinson GN, Hayden CC, Shobatake K, Sparks RK, Schafer TP, Lee YT (1985) Molecular beam studies of the $F + D_2$ and F + HD reactions. J Chem Phys 82(7):3067
95. Park TJ, Light JC (1986) Unitary quantum time evolution by iterative Lanczos reduction. J Chem Phys 85:5870

96. Peng T, Zhang JZH (1996) A reactant-product decoupling method for state-to-state reactive scattering. J Chem Phys 105(14):6072
97. Polanyi JC, Schreiber JL (1974) Distribution of reaction products (theory). Investigation of an ab initio energy-surface for $F + H_2 \rightarrow HF + H$. Chem Phys Lett 29:319
98. Polanyi JC, Schreiber JL (1977) The reaction of $F + H_2 \rightarrow HF + H$. A case study in reaction dynamics. Faraday Discuss Chem Soc 62:267
99. Porter RN (1974) Molecular trajectory calculations. Annu Rev Phys Chem 25(1):317
100. Qiu M, Ren Z, Che L, Dai D, Harich SA, Wang X, Yang X, Xu C, Xie D, Gustafsson M, Skodje RT, Sun Z, Zhang DH (2006) Observation of feshbach resonances in the $F + H_2 \rightarrow HF + H$ reaction. Science 311(5766):1440
101. Rackham EJ, Gonzalez-Lezana T, Manolopoulos DE (2003) A rigorous test of the statistical model for atomdiatom insertion reactions. J Chem Phys 119(24):12895
102. Ren ZF, Che L, Qiu MH, Wang XA, Dong WR, Dai DX, Wang XY, Yang XM, Sun ZG, Fu B, Lee SY, Xu X, Zhang DH (2008) Probing the resonance potential in the f atom reaction with hydrogen deuteride with spectroscopic accuracy. Proc Natl Acad Sci USA 105(35):12662
103. Rice J, Baronavski A (1991) Nonstatistical CO product distributions from the hot H-atom reaction, $H + CO_2 \rightarrow OH + CO$. J Chem Phys 94:1006
104. Sadeghi R, Skodje RT (1994) Barriers, thresholds, and resonances: spectral quantization of the transition state for the collinear $D + H_2$ reaction. J Chem Phys 102(1):193
105. Schaefer TP, Siska PE, Parson JM, Tully FP, Wong YC, Lee Y (1970) Crossed molecular beam study of $F + D_2$. J Chem Phys 53(8):3385
106. Schatz GC (1973) Large quantum effects in the collinear $F + H_2 \rightarrow FH + H$ reaction. J Chem Phys 58(9):4023
107. Schatz GC (1996) Scattering theory and dynamics: time-dependent and time-independent methods. J Phys Chem 100:12839
108. Schatz GC, Kuppermann A (1973) Role of direct and resonant (compound state) processes and of their interferences in the quantum dynamics of the collinear $H + H_2$ exchange reaction. J Chem Phys 59(2):964
109. Schatz G, Kuppermann A (1975) Dynamical resonances in collinear, coplanar, and three-dimensional quantum mechanical reactive scattering. Phys Rev Lett 35(19):1266
110. Schatz GC, Kuppermann A (1976) Quantum mechanical reactive scattering for three-dimensional atom plus diatom systems. I. Theory. J Chem Phys 65(11):4642
111. Schatz GC, Kuppermann A (1976) Quantum mechanical reactive scattering for three-dimensional atom plus diatom systems. II. Accurate cross sections for $H + H_2$. J Chem Phys 65(11):4668
112. Schatz GC, Bowman JM, Kuppermann A (1975) Exact quantum, quasiclassical, and semi-classical reaction probabilities for the collinear $F + H_2 \rightarrow FH + H$ reaction. J Chem Phys 63(2):674
113. Schatz GC, Bowman JM, Kuppermann A (1975) Exact quantum, quasiclassical, and semi-classical reaction probabilities for the collinear $F + D_2 \rightarrow FD + D$ reaction. J Chem Phys 63(2):685
114. Schatz G, Fitzcharles M, Harding L (1987) State-to-state chemistry with fast hydrogen atoms. Faraday Discuss 84:359
115. Schrödinger E (1926) Quantisierung als eigenwert problem. Ann Phys 79:361
116. Skodje RT, Skouteris D, Manolopoulos DE, Lee SH, Dong F, Liu K (2000) Observation of a transition state resonance in the integral cross section of the $F + HD$ reaction. J Chem Phys 112(10):4536
117. Skodje R, Skouteris D, Manolopoulos D, Lee SH, Dong F, Liu K (2000) Resonance-mediated chemical reaction: $F + HD \rightarrow HF + D$. Phys Rev Lett 85(6):1206
118. Skokov S, Bowman J (2001) State-to-state reactive scattering via real I^2 wave packet propagation for reduced dimensionality $AB + CD$ reactions. J Phys Chem A 105:2502–2508
119. Skouteris D, Castillo JF, Manolopoulos DE (2000) Abc: a quantum reactive scattering program. Comput Phys Commun 133(1):128–135

120. Smith IWM (1990) Vibrational adiabaticity in chemical reactions. Acc Chem Res 23(4):101
121. Stark K, Werner HJ (1996) An accurate multireference configuration interaction calculation of the potential energy surface for the $F + H_2 \rightarrow HF + H$ reaction. J Chem Phys 104(17):6515
122. Steckler R, Truhlar DG, Garrett BC (1985) A highbarrier potential energy surface for $F + H_2 \rightarrow HF + H$. J Chem Phys 83(6):2870
123. Strazisar B, Lin C, Davis H (2000) Mode-specific energy disposal in the four-atom reaction $OH + D_2 \rightarrow HOD + D$. Science 290:958
124. Sun Z, Zhang DH, Xu C, Zhou S, Xie D, Lendvay G, Lee SY, Lin SY, Guo H (2008) State-to-state dynamics of $H + O_2$ reaction, evidence for nonstatistical behavior. J Am Chem Soc 130(45):14962
125. Sun Z, Lee SY, Guo H, Zhang DH (2009) Comparison of second-order split operator and chebyshev propagator in wave packet based state-to-state reactive scattering calculations. J Chem Phys 130(17):174102
126. Sun Z, Lin X, Lee SY, Zhang DH (2009) A reactant-coordinate-based time-dependent wave packet method for triatomic state-to-state reaction dynamics: application to the $H + O_2$ reaction. J Phys Chem A 113(16):4145
127. Sun Z, Guo H, Zhang DH (2010) Extraction of state-to-state reactive scattering attributes from wave packet in reactant jacobi coordinates. J Chem Phys 132(8):084112
128. Sun Z, Liu L, Lin SY, Schinke R, Guo H, Zhang DH (2010) State-to-state quantum dynamics of $O + O_2$ isotope exchange reactions reveals nonstatistical behavior at atmospheric conditions. Proc Natl Acad Sci USA 107(2):555
129. Sun ZG, Zhang DH, Alexander MH (2010) Time-dependent wavepacket investigation of state-to-state reactive scattering of Cl with $para$-H_2 including the open-shell character of the cl atom. J Chem Phys 132(3):034308
130. Sun Z, Yang W, Zhang DH (2012) Higher-order split operator schemes for solving the Schrödinger equation in the time-dependent wave packet method: applications to triatomic reactive scattering calculations. Phys Chem Chem Phys 14:1827
131. Tal-Ezer H, Kosloff R (1984) An accurate and efficient scheme for propagating the time dependent Schrödinger equation. J Chem Phys 81:3967
132. Tannor DJ, Weeks DE (1993) Wave packet correlation function formulation of scattering theory: the quantum analog of classical s-matrix theory. J Chem Phys 98(5):3884
133. Truhlar DG (1972) Exact and approximate quantum mechanical reaction probabilities and rate constants for the collinear $H + H_2$ reaction. J Chem Phys 56(5):2232
134. Truhlar DG, Kuppermann A (1970) Quantum mechanics of the $h + h_2$ reaction: exact scattering probabilities for collinear collisions. J Chem Phys 52(7):3841
135. Truhlar DG, Garrett BC, Blais NC (1984) Two new potential energy surfaces for the $F + H_2$ reaction. J Chem Phys 80(1):232
136. Truhlar DG, Garrett BC, Klippenstein SJ (1996) Current status of transition-state theory. J Phys Chem 100(31):12771
137. Truong TN, Tanner JJ, Bala P, McCammon JA, Kouri DJ, Lesyng B, Hoffman DK (1991) A comparative study of time dependent quantum mechanical wave packet evolution methods. J Chem Phys 96:2077
138. Valero R, McCormack D, Kroes G (2004) New results for the $OH(v = 0, j = 0) + CO(v = 0, j = 0) \rightarrow H + CO_2$ reaction: five-and full-dimensional quantum dynamical study on several potential energy surfaces. J Chem Phys 120:4263
139. Wang XA, Dong WR, Qiu MH, Ren ZF, Che L, Dai DX, Wang XY, Yang XM, Sun ZG, Fu B, Lee SY, Xu X, Zhang DH (2008) Hf(v = 3) forward scattering in the $F + H_2$ reaction: shape resonance and slow-down mechanism. Proc Natl Acad Sci USA 105(17):6227
140. Wang XG, Dong WR, Xiao CL, Che L, Ren ZF, Dai DX, Wang XY, Casavecchia P, Yang XM, Jiang B, Xie DQ, Sun ZG, Lee SY, Zhang DH, Werner HJ, Alexander MH (2008) The extent of non-born-oppenheimer coupling in the reaction of $Cl(P_2)$ with $para$-H_2. Science 322(5901):573

141. Wang T, Yang TG, Xiao CL, Dai DX, Yang XM (2013) Highly efficient pumping of vibrationally excited HD molecules via stark-induced adiabatic Raman passage. J Phys Chem Lett 4:368
142. Warnatz J (1984) Combustion chemistry. Springer, New York
143. Wu SF, Levine RD (1971) Quantum mechanical computational studies of chemical reactions: I. Close-coupling method for the collinear $H + H_2$ reaction. Mol Phys 22(5):881
144. Wu SF, Johnson BR, Levine RD (1973) Quantum mechanical computational studies of chemical reactions: III. Collinear a + bc reaction with some model potential energy surfaces. Mol Phys 25(4):839
145. Xiao CL, Xu X, Liu S, Wang T, Dong WR, Yang TG, Sun ZG, Dai DX, Xu X, Zhang DH, Yang XM (2011) Experimental and theoretical differential cross sections for a four-atom reaction: $HD + OH \rightarrow H_2O + D$. Science 333(6041):440
146. Xie D, Chen R, Guo H (2000) Comparison of Chebyshev, Faber, and Lanczos propagation-based methods for calculating resonances. J Chem Phys 112:5263
147. Yang X (2005) State-to-state dynamics of elementary chemical reactions using rydberg h-atom translational spectroscopy. Int Rev Phys Chem 24(1):37
148. Yang X, Zhang DH (2008) Dynamical resonances in the fluorine atom reaction with the hydrogen molecule. Acc Chem Res 41(8):981
149. Yu H, Nyman G (2000) Interpolated ab initio quantum scattering for the reaction of oh with hcl. J Chem Phys 113:8936
150. Yu H, Muckerman J, Sears T (2001) A theoretical study of the potential energy surface for the reaction OH + CO. Chem Phys Lett 349:547
151. Yuan K, Cheng Y, Liu X, Harich S, Yang X, Zhang D (2006) Experimental and quantum dynamical study on an asymmetric insertion reaction: state-to-state dynamics of $O(^1D) + HD(^1\Sigma_g^+, v = 0, j = 0) \rightarrow OH(^2\Pi, v, N) + D(^2S)$. Phys Rev Lett 96(10):103202
152. Zare RN (1988) Angular momentum: understanding spatial aspects in chemistry and physics. Wiley, New York
153. Zhang JZH (1999) Theory and application of quantum molecular dynamics. World Scientific, River Edge
154. Zhang D (2006) State-to-state quantum reactive scattering for four-atom chemical reactions: differential cross section for the $H + H_2O \rightarrow H_2 + OH$ abstraction reaction. J Chem Phys 125:133102
155. Zhang D, Lee S (1999) Fully converged integral cross sections of diatom-diatom reactions and the accuracy of the centrifugal sudden approximation in the $H_2 + OH$ reaction. J Chem Phys 110:4435
156. Zhang DH, Light JC (1996) Quantum state-to-state reaction probabilities for the $H + H_2O \rightarrow H_2 + OH$ reaction in six dimensions. J Chem Phys 105(3):1291
157. Zhang JZH, Miller WH (1989) Quantum reactive scattering via the s-matrix version of the kohn variational principle: differential and integral cross sections for $D + H_2 \rightarrow HD + H$. J Chem Phys 91(3):1528
158. Zhang D, Zhang J (1993) Accurate quantum calculation for the benchmark reaction $H_2 + OH \rightarrow H_2O + H$ in five-dimensional space: reaction probabilities for $J = 0$. J Chem Phys 99:5615
159. Zhang D, Zhang J (1994) Full-dimensional time-dependent treatment for diatom-diatom reactions: the $H_2 + OH$ reaction. J Chem Phys 101:1146
160. Zhang DH, Zhang JZH (1994) Quantum reactive scattering with a deep well: time-dependent calculation for $H + O_2$ reaction and bound state characterization for HO_2. J Chem Phys 101(5):3671
161. Zhang D, Zhang J, Light J (1996) A six dimensional quantum study for atom-triatom reactions: the $H + H_2O \rightarrow H_2 + OH$ reaction. J Chem Phys 104:4544
162. Zhang D, Collins M, Lee S (2000) First-principles theory for the $H + H_2O$, D_2O reactions. Science 290:961
163. Zhang D, Xie D, Yang M, Lee S (2002) State-to-state integral cross section for the $H + H_2O \rightarrow H_2 + OH$ abstraction reaction. Phys Rev Lett 89:283203

164. Zhang D, Yang M, Lee S (2003) Accuracy of the centrifugal sudden approximation in the $H + H_2O$ reaction and accurate integral cross sections for the $H + H_2O \rightarrow H_2 + OH$ abstraction reaction. J Chem Phys 117:10067
165. Zhu W, Dai J, Zhang J, Zhang D (1996) State-to-state time-dependent quantum calculation for reaction $H_2 + OH \rightarrow H_2O + H$ in six dimensions. J Chem Phys 105:4881
166. Zhu W, Zhang JZH, Zhang YC, Zhang YB, Zhan LX, Zhang SL, Zhang DH (1998) Quantum dynamics study of $H_2 + CN \rightarrow HCN + H$ reaction in full dimensions. J Chem Phys 108:3509